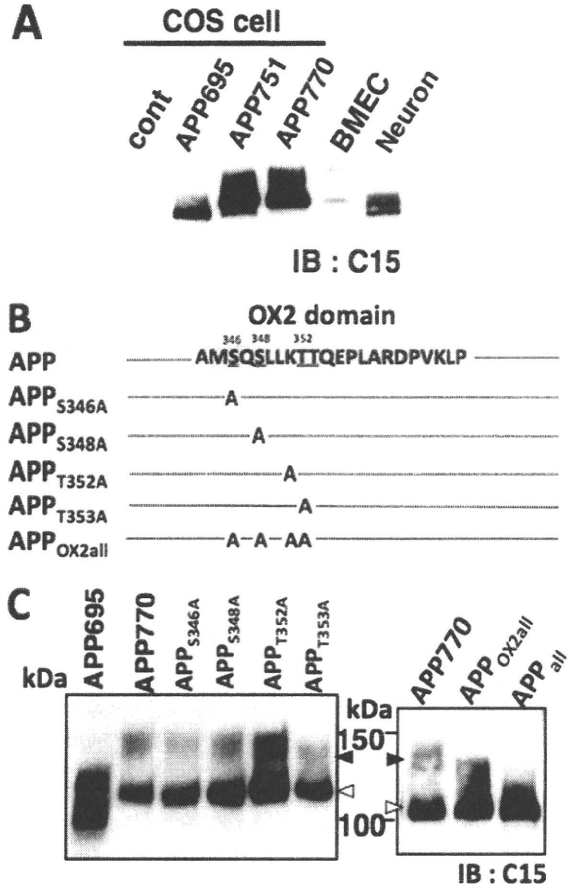

FIGURE 3. **Analysis of a series of APP770 mutants.** *A*, human APP695, APP751, and APP770 were individually overexpressed in COS cells. The obtained cell lysates (1 μg of protein) together with lysates of BMECs (5 μg of protein) and neurons (10 μg of protein) were analyzed by Western blotting with the anti-APP C15 antibody. *B*, schematic diagrams of the APP770 mutants used in this study. *C*, wild-type APP770 or its mutants were expressed in COS cells and subjected to Western blot analysis with the anti-APP C15 antibody. The *black* and *gray arrowheads* show APP-H and APP-L, respectively. *cont*, control; *IB*, immunoblot.

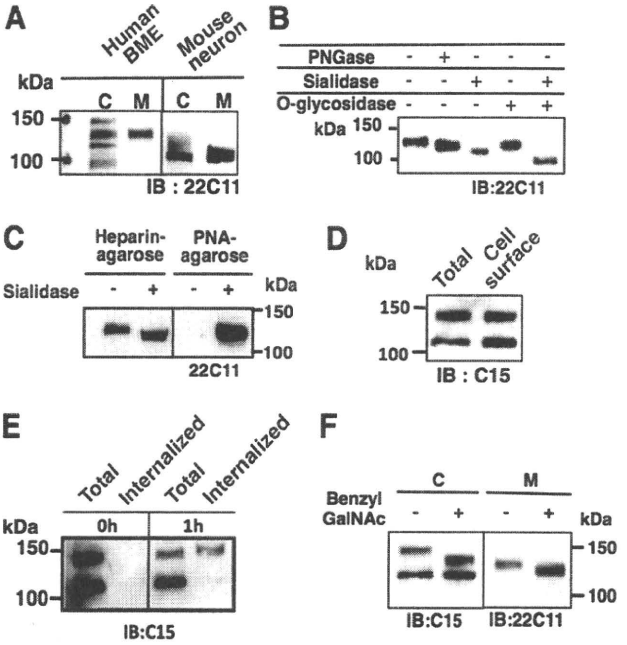

FIGURE 4. **Characterization of sAPP secreted from BMECs.** *A*, intact APP in cell lysates (6 μg) and soluble secreted sAPP pulled-down with heparin-agarose from the media of BMECs and mouse primary neurons were analyzed by Western blotting with the anti-APP 22C11 antibody. *C*, cell lysates; *M*, media. *B*, sAPP pulled down with heparin-agarose from the BMEC media was incubated in the presence or absence of sialidase and *O*-glycosidase and then analyzed by immunoblotting (*IB*) with the anti-APP 22C11 antibody. *C*, media from BMEC cultures (0.5 ml) were incubated in the presence or absence of *Arthrobacter ureafaciens* sialidase (4 milliunits) for 18 h. The digested samples were incubated with heparin-agarose or PNA agarose (20 μl each). The precipitated samples were analyzed by Western blotting with the anti-APP 22C11 antibody. *D*, following cell-surface biotinylation of BMECs, biotinylated cell surface proteins were precipitated with streptavidin-Sepharose and then analyzed by Western blotting with the anti-APP C15 antibody. *E*, after cell-surface labeling of BMECs using NHS-SS-biotin, the cells were incubated for 0 or 1 h to allow internalization of the biotinylated proteins. Cell surface biotin was then stripped by reductive treatment. Total proteins, or internalized biotinylated proteins that were precipitated with streptavidin-Sepharose, were analyzed by Western blotting with the anti-APP C15 antibody. *F*, BMECs were cultured in the presence of benzyl GalNAc, and then intact APP and sAPP were analyzed by Western blotting with the anti-APP C15 and 22C11 antibodies, respectively.

O-Glycosylated APP770 Is Preferentially Secreted to Media—Next, we analyzed the APP metabolites in endothelial cells. We performed Western blot analyses of BMEC lysates and culture media with the anti-APP 22C11 antibody, which recognizes the N-terminal APP region and therefore detects sAPP. We observed three bands in the cell lysates using the anti-22C11 antibody. In the media, we detected a single sAPP band that migrated with the middle band observed in the cell lysates (Fig. 4*A*), suggesting that sAPP is solely derived from APP-H. Indeed, sAPP was sensitive to both sialidase and *O*-glycosidase treatments (Fig. 4*B*). Furthermore, after sialidase treatment, most of the sAPP was precipitated with PNA lectin (Fig. 4*C*), indicating that sAPP mostly contains sialylated core 1 type *O*-glycan chains. It should be noted that we failed to detect sAPP without *O*-glycans. Considering that APP cleavage at the α-site seems to occur at the cell surface, whereas cleavage at the β-site occurs during the endocytotic pathway (24), it is possible that APP without *O*-glycosylation is unable to move to the cell surface to encounter either α- or β-secretase. However, cell surface biotinylation experiments showed that both APP-H and APP-L reached the cell surface (Fig. 4*D*). We next studied how cell surface APP is metabolized in the cell. To analyze APP internalization, we next labeled the surface of BMECs with a disulfide cleavable biotinylation reagent (19). Internalization was then induced at 37 °C for 1 h. Interestingly, we found that only APP-H was endocytosed (Fig. 4*E*). This suggests that cell surface APP-H uses a specific intracellular trafficking pathway to encounter both α- and β-secretase. Furthermore, benzyl GalNAc, an inhibitor of *O*-glycan chain elongation, failed to inhibit sAPP secretion into the media (Fig. 4*F*).

Aβ is Produced from Brain Endothelial Cells—Since there is limited information regarding the expression levels and activities of the endothelial α-secretase and β-secretase enzymes for the processing of APP770, we characterized the soluble sAPP770 secreted from BMECs. Using specific antibodies against sAPPα and sAPPβ, we successfully detected both sAPP770α and sAPP770β (Fig. 5*A*). Since the amyloidogenic β-secretase pathway is present in endothelial cells, it is rea-

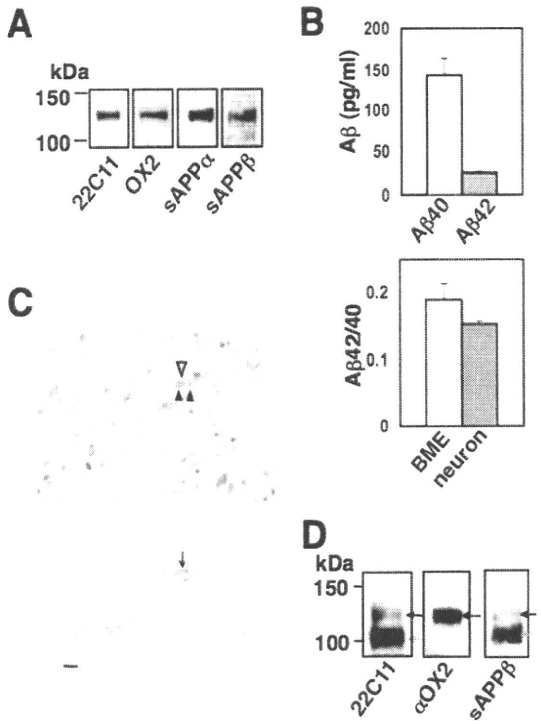

FIGURE 5. **Analysis of APP770 in the human brain.** *A*, sAPP770 secreted from BMECs was analyzed by Western blotting with anti-APP 22C1, anti-OX2, anti-sAPPα, and anti-sAPPβ antibodies. *B*, culture media from BMECs cultured in Opti-MEM were analyzed for their levels of Aβ40 and Aβ42 (n = 3; *upper panel*). The ratios of Aβ42/Aβ40 secreted from BMECs and neurons are shown as the means ± S.E. (n = 4) (*lower panel*). *C*, paraffin-embedded human cerebral sections were analyzed by hematoxylin-eosin staining (*upper panel*) and immunostaining with the anti-OX2 antibody (*lower panel*). The *gray* and *black arrowheads* show the nuclei of endothelial cells and smooth muscle cells, respectively. The *arrow* shows the OX2-immunoreactive endothelium. *Scale bar*, 20 μm. *D*, sAPP in human CSF samples (0.5 ml each) was pulled down with heparin-agarose (30 μl) and then analyzed by Western blotting with anti-APP 22C11, anti-sAPPβ, and anti-OX2 antibodies.

sonable to consider that these cells also have γ-secretase activity to produce Aβ peptides. Even though endogenous Aβ was not detectable, we detected both Aβ40 and Aβ42 in the culture media of BMECs overexpressing APP770, and the ratio of endothelial Aβ42/Aβ40 was similar to that in neurons (Fig. 5*B*).

APP770 is Expressed in Cerebral Vessels and sAPP770β Is Secreted into the CSF—To clarify whether APP770 is indeed expressed in cerebral vessels, we first analyzed cerebral cortex sections with an anti-OX2 antibody to determine the localization of APP770. The luminal regions of the venous and venular endothelial cells, but not smooth muscle cells, were stained with the anti-OX2 antibody (Fig. 5*C*). No immunohistochemical signals were observed in the vessels of the arachnoid. Next, we investigated whether the CSF contains sAPP770β, the N-terminal β-secretase cleavage product of APP770. sAPP was pulled-down from CSF using heparin-agarose and then immunostained with anti-APP 22C11, anti-OX2 and anti-sAPPβ antibodies. We detected two bands with the anti-APP 22C11 antibody, of which only the upper band was detected with the anti-OX2 antibody (Fig. 5*D*), indicating that the upper band is derived from APP770. Since both the upper and lower bands were detected with the anti-sAPPβ antibody, both forms contain β-secretase cleavage products.

DISCUSSION

The dementia of AD is closely associated with accumulation of Aβ in the brain parenchyma and in the walls of blood vessels in the brain (25–27). Aβ deposition in the cerebral vasculature contributes to cerebral amyloid angiopathy, which shows a prevalence of >80% among AD individuals and 10–40% in elderly people without AD (28). Microbleeds in the brain occur in most cerebral amyloid angiopathy cases (25). Although important roles for cerebral vascular smooth muscle cells in vascular Aβ clearance were recently highlighted (29), the regions where vascular Aβ is produced for deposition remain to be determined.

We have shown for the first time that brain endothelial cells express APP770. First, we unambiguously detected APP770 expression in human BMECs. Using an anti-APP770 antibody that recognizes the OX2 domain for immunohistochemical staining of the cerebral cortex, we found that APP770 was expressed in venous and venular endothelial cells. We also showed that Aβ40 and Aβ42 were produced in BMECs. Therefore, our study points out the possibility that endothelial Aβ peptides could be the source of the Aβ deposits in cerebral vessel walls. Even though our immunohistochemical study is somewhat different from the previous observations in which Aβ deposits are frequently found in cortical arteries, the major distribution of APP770 in the brain might be different from where Aβ is mainly produced from APP770 to cause vascular Aβ deposits.

Perdivara *et al.* (16) recently identified the core 1 type *O*-glycans attached to residues Thr291, Thr292 and Thr576 of APP695. Here, we have shown that APP770 has an additional *O*-glycan chain at residue Thr353 within the OX2 domain. Furthermore, a series of site-directed mutations within the KPI domain had no effect on the mobility of APP770 (Fig. S3), indicating the absence of *O*-glycans in the KPI domain. A large ectodomain of APP consists of several subdomains, such as the E1 (30), E2 (31), and KPI domains (32). The web application POODLE-S (Prediction of Order and Disorder by Machine Learning) predicts that the other regions, in which all of the *O*-glycans are located, are intrinsically unstructured (33) (supplemental Fig. S4). Therefore, it is unlikely that the addition of any *O*-glycans to APP770 would result in conformational changes that might affect the α- or β-secretase cleavage. Because we found that *O*-glycosylated APP is selectively internalized, how *O*-glycosylation of APP would modulate its intracellular trafficking to the same intracellular compartment as α- and β-secretase remains an interesting and unanswered question. Because APP695 was also shown to contain *O*-glycans, whether our finding applies to neuronal APP also remains to be resolved. We found that BMECs expressed higher amounts of *O*-glycosylated APP770 than did COS cells, suggesting that endothelial cells possess a highly developed *O*-glycosylation machinery. Interestingly, endothelial *O*-glycan deficiency causes blood/lymphatic misconnections (34), indicating a fundamental role for *O*-glycans in vascular development.

In this study, we were able to discriminate CSF sAPP770β from other types of sAPPβ. As BACE1 seems to be a stress-response protein (35), one of our ongoing projects is elucidation of the critical factors required to increase sAPP770β secretion. We are now establishing a sandwich ELISA system to quantify sAPP770β in CSF or plasma. Because the CSF sAPP770β appears to be mainly derived from brain endothelial cells, sAPP770β would be a potential biomarker for diagnosing cerebrovascular dementia or AD.

Acknowledgments—We thank Dr. Shoichi Ishiura (The University of Tokyo) for the human APP751 and APP770 pcDNAs and Dr. Kei Maruyama (Saitama Medical School) for the anti-APP C15 antibody. We also thank Dr. Makoto Higuchi (National Institute of Radiological Sciences) for valuable discussions.

REFERENCES

1. Selkoe, D. J. (2001) *Physiol. Rev.* **81,** 741–766
2. Tanzi, R. E., and Bertram, L. (2005) *Cell* **120,** 545–555
3. Yan, R., Bienkowski, M. J., Shuck, M. E., Miao, H., Tory, M. C., Pauley, A. M., Brashier, J. R., Stratman, N. C., Mathews, W. R., Buhl, A. E., Carter, D. B., Tomasselli, A. G., Parodi, L. A., Heinrikson, R. L., and Gurney, M. E. (1999) *Nature* **402,** 533–537
4. Vassar, R., Bennett, B. D., Babu-Khan, S., Kahn, S., Mendiaz, E. A., Denis, P., Teplow, D. B., Ross, S., Amarante, P., Loeloff, R., Luo, Y., Fisher, S., Fuller, J., Edenson, S., Lile, J., Jarosinski, M. A., Biere, A. L., Curran, E., Burgess, T., Louis, J. C., Collins, F., Treanor, J., Rogers, G., and Citron, M. (1999) *Science* **286,** 735–741
5. Sinha, S., Anderson, J. P., Barbour, R., Basi, G. S., Caccavello, R., Davis, D., Doan, M., Dovey, H. F., Frigon, N., Hong, J., Jacobson-Croak, K., Jewett, N., Keim, P., Knops, J., Lieberburg, I., Power, M., Tan, H., Tatsuno, G., Tung, J., Schenk, D., Seubert, P., Suomensaari, S. M., Wang, S., Walker, D., Zhao, J., McConlogue, L., and John, V. (1999) *Nature* **402,** 537–540
6. Wolfe, M. S., Xia, W., Ostaszewski, B. L., Diehl, T. S., Kimberly, W. T., and Selkoe, D. J. (1999) *Nature* **398,** 513–517
7. De Strooper, B., Annaert, W., Cupers, P., Saftig, P., Craessaerts, K., Mumm, J. S., Schroeter, E. H., Schrijvers, V., Wolfe, M. S., Ray, W. J., Goate, A., and Kopan, R. (1999) *Nature* **398,** 518–522
8. Beher, D., Hesse, L., Masters, C. L., and Multhaup, G. (1996) *J. Biol. Chem.* **271,** 1613–1620
9. Small, D. H., Nurcombe, V., Moir, R., Michaelson, S., Monard, D., Beyreuther, K., and Masters, C. L. (1992) *J Neurosci.* **12,** 4143–4150
10. Reinhard, C., Hébert, S. S., and De Strooper, B. (2005) *EMBO J.* **24,** 3996–4006
11. Herms, J., Anliker, B., Heber, S., Ring, S., Fuhrmann, M., Kretzschmar, H., Sisodia, S., and Müller, U. (2004) *EMBO J.* **23,** 4106–4115
12. Ponte, P., Gonzalez-DeWhitt, P., Schilling, J., Miller, J., Hsu, D., Greenberg, B., Davis, K., Wallace, W., Lieberburg, I., and Fuller, F. (1988) *Nature* **331,** 525–527
13. Tanzi, R. E., McClatchey, A. I., Lamperti, E. D., Villa-Komaroff, L., Gusella, J. F., and Neve, R. L. (1988) *Nature* **331,** 528–530
14. Wertkin, A. M., Turner, R. S., Pleasure, S. J., Golde, T. E., Younkin, S. G., Trojanowski, J. Q., and Lee, V. M. (1993) *Proc. Natl. Acad. Sci. U.S.A.* **90,** 9513–9517
15. Xu, F., Davis, J., Miao, J., Previti, M. L., Romanov, G., Ziegler, K., and Van Nostrand, W. E. (2005) *Proc. Natl. Acad. Sci. U.S.A.* **102,** 18135–18140
16. Perdivara, I., Petrovich, R., Allinquant, B., Deterding, L. J., Tomer, K. B., and Przybylski, M. (2009) *J. Proteome Res.* **8,** 631–642
17. Kitazume, S., Imamaki, R., Ogawa, K., Komi, Y., Futakawa, S., Kojima, S., Hashimoto, Y., Marth, J. D., Paulson, J. C., and Taniguchi, N. (2010) *J. Biol. Chem.* **285,** 6515–6521
18. Hama, E., Shirotani, K., Masumoto, H., Sekine-Aizawa, Y., Aizawa, H., and Saido, T. C. (2001) *J. Biochem.* **130,** 721–726
19. Aroeti, B., and Mostov, K. E. (1994) *EMBO J.* **13,** 2297–2304
20. Koo, E. H., Sisodia, S. S., Archer, D. R., Martin, L. J., Weidemann, A., Beyreuther, K., Fischer, P., Masters, C. L., and Price, D. L. (1990) *Proc. Natl. Acad. Sci. U.S.A.* **87,** 1561–1565
21. Palmert, M. R., Podlisny, M. B., Witker, D. S., Oltersdorf, T., Younkin, L. H., Selkoe, D. J., and Younkin, S. G. (1989) *Proc. Natl. Acad. Sci. U.S.A.* **86,** 6338–6342
22. Sato, Y., Liu, C., Wojczyk, B. S., Kobata, A., Spitalnik, S. L., and Endo, T. (1999) *Biochim Biophys Acta.* **1472,** 344–358
23. Tomita, S., Kirino, Y., and Suzuki, T. (1998) *J. Biol. Chem.* **273,** 6277–6284
24. Ehehalt, R., Keller, P., Haass, C., Thiele, C., and Simons, K. (2003) *J. Cell. Biol.* **160,** 113–123
25. Vonsattel, J. P., Myers, R. H., Hedley-Whyte, E. T., Ropper, A. H., Bird, E. D., and Richardson, E. P., Jr. (1991) *Ann. Neurol.* **30,** 637–649
26. Van Broeckhoven, C., Haan, J., Bakker, E., Hardy, J. A., Van Hul, W., Wehnert, A., Vegter-Van der Vlis, M., and Roos, R. A. (1990) *Science* **248,** 1120–1122
27. Rovelet-Lecrux, A., Hannequin, D., Raux, G., Le Meur, N., Laquerrière, A., Vital, A., Dumanchin, C., Feuillette, S., Brice, A., Vercelletto, M., Dubas, F., Frebourg, T., and Campion, D. (2006) *Nat. Genet.* **38,** 24–26
28. Greenberg, S. M., Gurol, M. E., Rosand, J., and Smith, E. E. (2004) *Stroke* **35,** 2616–2619
29. Bell, R. D., Deane, R., Chow, N., Long, X., Sagare, A., Singh, I., Streb, J. W., Guo, H., Rubio, A., Van Nostrand, W., Miano, J. M., and Zlokovic, B. V. (2009) *Nat. Cell. Biol.* **11,** 143–153
30. Dahms, S. O., Hoefgen, S., Roeser, D., Schlott, B., Gührs, K. H., and Than, M. E. (2010) *Proc. Natl. Acad. Sci. U.S.A.* **107,** 5381–5386
31. Wang, Y., and Ha, Y. (2004) *Mol. Cell.* **15,** 343–353
32. Hynes, T. R., Randal, M., Kennedy, L. A., Eigenbrot, C., and Kossiakoff, A. A. (1990) *Biochemistry* **29,** 10018–10022
33. Shimizu, K., Hirose, S., and Noguchi, T. (2007) *Bioinformatics* **23,** 2337–2338
34. Fu, J., Gerhardt, H., McDaniel, J. M., Xia, B., Liu, X., Ivanciu, L., Ny, A., Hermans, K., Silasi-Mansat, R., McGee, S., Nye, E., Ju, T., Ramirez, M. I., Carmeliet, P., Cummings, R. D., Lupu, F., and Xia, L. (2008) *J. Clin. Invest.* **118,** 3725–3737
35. Vassar, R., Kovacs, D. M., Yan, R., and Wong, P. C. (2009) *J. Neurosci.* **29,** 12787–12794

JOURNAL OF VIROLOGY, May 2009, p. 4995–5004
0022-538X/09/$08.00+0 doi:10.1128/JVI.02225-08

Vol. 83, No. 10

Receptor-Dependent and -Independent Axonal Retrograde Transport of Poliovirus in Motor Neurons▽†

Seii Ohka,[1]* Mai Sakai,[1] Stephanie Bohnert,[2] Hiroko Igarashi,[1] Katrin Deinhardt,[2]‡ Giampietro Schiavo,[2] and Akio Nomoto[1]

Department of Microbiology, Graduate School of Medicine, The University of Tokyo, 7-3-1 Hongo, Bunkyo-ku, Tokyo 113-0033, Japan,[1] and Molecular NeuroPathobiology Laboratory, Cancer Research UK London Research Institute, Lincoln's Inn Fields Laboratories, 44 Lincoln's Inn Fields, London WC2A 3PX, United Kingdom[2]

Received 22 October 2008/Accepted 18 February 2009

Poliovirus (PV), when injected intramuscularly into the calf, is incorporated into the sciatic nerve and causes an initial paralysis of the inoculated limb in transgenic (Tg) mice carrying the human PV receptor (hPVR/CD155) gene. We have previously demonstrated that a fast retrograde axonal transport process is required for PV dissemination through the sciatic nerves of hPVR-Tg mice and that intramuscularly inoculated PV causes paralytic disease in an hPVR-dependent manner. Here we showed that hPVR-independent axonal transport of PV was observed in hPVR-Tg and non-Tg mice, indicating that several different pathways for PV axonal transport exist in these mice. Using primary motor neurons (MNs) isolated from these mice or rats, we demonstrated that the axonal transport of PV requires several kinetically different motor machineries and that fast transport relies on a system involving cytoplasmic dynein. Unexpectedly, the hPVR-independent axonal transport of PV was not observed in cultured MNs. Thus, PV transport machineries in cultured MNs and in vivo differ in their hPVR requirements. These results suggest that the axonal trafficking of PV is carried out by several distinct pathways and that MNs in culture and in the sciatic nerve in situ are intrinsically different in the uptake and axonal transport of PV.

In humans, paralytic poliomyelitis results from the invasion of the central nervous system by circulating poliovirus (PV), probably via the blood-brain barrier. This conclusion is supported by the finding that circulating PV after intravenous inoculation in mice appears to cross the blood-brain barrier at a high rate in a human PV receptor (hPVR/CD155)-independent manner (44). After the virus enters the central nervous system, it replicates in neurons, especially in motor neurons (MNs), inducing the cell death that causes paralytic poliomyelitis. Along with this route of dissemination, a neuron-specific pathway has been reported in humans (31), monkeys (18), and PV-sensitive transgenic (Tg) mice carrying the hPVR gene (34, 37). This neuron-specific pathway appears to be important in causing "provocation poliomyelitis," which is triggered by injuries after PV ingestion (11). Using differentiated PC12 cells and a PV-sensitive Tg mouse line, we have shown that intramuscularly inoculated PV is taken up by endocytosis at synapses.

hPVR is a member of the immunoglobulin (Ig) superfamily, with three linked extracellular Ig-like domains, followed by a membrane-spanning domain and a cytoplasmic domain. Two membrane-bound forms (α and δ) and two secreted forms (β and γ) of hPVR derived by alternative splicing are likely to be expressed in human cells (23). Membrane-bound hPVRs are considered to play important roles in the early steps of infection, such as the binding of the virus to the cell surface, its entry into the cell, and the uncoating of the virus. The N-terminal Ig-like domain harbors the sites for PV binding, and anti-hPVR monoclonal antibodies (MAbs) directed against this region block PV infection (9, 24, 39).

hPVR has the ability to alter the conformation of PV from the 160S intact infectious particle to a 135S particle from which the viral capsid protein VP4 is missing (2, 29). PV-related materials recovered from the sciatic nerves of PV-sensitive Tg mice after intramuscular inoculation with PV were mainly composed of intact 160S virions. The amount of 160S particles recovered was greatly reduced by coinjection with MAb p286, which specifically recognizes hPVR (34). Thus, most of the intramuscularly inoculated PV is incorporated into the sciatic nerves of PV-sensitive Tg mice as intact particles in an hPVR-dependent manner. This surprising finding might be due to either of two alternative, yet not mutually exclusive, possibilities: (i) a small number of PVRs bound per virion does not result in a conformational change in the viral capsid with a loss of VP4, but it is sufficient to induce endocytosis of the virus on the cell surface, or (ii) a cellular inhibitor(s) of PV uncoating may exist in the endocytic pathway responsible for PV uptake and transport in Tg mice (34).

This mouse strain also allowed us to demonstrate that PV inoculated into the calf was incorporated into the sciatic nerve and retrogradely transported through the axons as intact virion particles. Furthermore, PV dissemination via the neural pathway has been found to rely on a fast retrograde axonal transport system and was inhibited by MAb p286 (34). Moreover,

* Corresponding author. Mailing address: Department of Microbiology, Graduate School of Medicine, The University of Tokyo, 7-3-1 Hongo, Bunkyo-ku, Tokyo 113-0033, Japan. Phone: 81-3-5841-3407. Fax: 81-3-5841-3374. E-mail: seii@m.u-tokyo.ac.jp.

† Supplemental material for this article may be found at http://jvi.asm.org/.

‡ Present address: Molecular Neurobiology Program, Skirball Institute of Biomolecular Medicine, New York University School of Medicine, New York, NY 10016.

▽ Published ahead of print on 25 February 2009.

the efficient direct interaction of the hPVR cytoplasmic domain with Tctex-1, a light chain of cytoplasmic dynein (21), has been suggested to play an important role in retrograde transport, together with microtubule integrity (33). Cytoplasmic dynein, a minus-end-directed microtubule-based motor complex (13, 14, 17, 43), is implicated in the transport of early and late endosomes, lysosomes, synaptic vesicles, and endoplasmic reticulum along microtubules (1, 8, 13, 14, 17, 43). Notwithstanding the recent progress in the understanding of PV trafficking, the molecular determinants of the axonal transport of PV in MNs have not yet been elucidated.

Despite the importance of axonal retrograde transport in health and disease, the direct visualization of retrograde transport and its quantitative analysis have been hampered by the lack of a reliable assay for living MNs. Such an assay was established in MNs by using a nontoxic fluorescent fragment of tetanus toxin (TeNT H_C), which binds to MNs and is retrogradely transported (28). Here, we applied this assay to the visualization of PV in living MNs.

We employed hPVR-Tg and non-Tg mice, together with cultured MNs isolated from these mice, to clarify the mechanisms of axonal retrograde transport of PV. Experiments involving cultured MNs showed that the entry and axonal transport of PV are strictly hPVR dependent. However, hPVR-independent axonal transport of PV can be observed in non-Tg as well as in hPVR-Tg mice, suggesting that multiple axonal transport routes for PV are present in vivo.

MATERIALS AND METHODS

Viruses and cells. The virulent Mahoney strain [PV1(M)OM] and the attenuated Sabin 1 strain [PV1(Sab)IC-0] of type 1 PV, derived from the infectious cDNA clones pOM1 (40) and pVS(1)IC-0(T) (22), respectively, were used in this study.

African green monkey kidney cells were grown in Dulbecco modified Eagle medium supplemented with 5% newborn calf serum and were used for the preparation of viruses, transfection experiments with the RNAs transcribed from infectious cDNA clones, and plaque assays. Suspension-cultured HeLa S3 cells were maintained in RPMI 1640 medium supplemented with 5% newborn calf serum and were used for preparation of [^{35}S]methionine-labeled or fluorescently labeled virus.

Rodents. IQI mice and their hPVR-Tg mouse line, IQI-PVRTg21 (25, 26), in the hemizygous stage were used as an animal model for studying the mechanisms of PV transport by the neural pathway. All mice were 6 to 10 weeks of age. For the preparation of MNs in culture (3, 12), embryonic day 14 (E14) Sprague-Dawley rat embryos or E13 IQI-PVRTg21 or C57BL/6-PVRTg21 mouse embryos were used. Mice and rats were treated according to the guidelines for the care and use of laboratory animals of the University of Tokyo. All mice and rats used were free from specific pathogens.

Antibodies. For PV immunohistochemistry in the sciatic nerve, 22.6 μg of mouse anti-hPVR MAb p286 (34) was intramuscularly coinjected with a virus suspension. In the case of coinjection with [^{35}S]methionine-labeled virus, as much as 42.2 μg of the MAb was added to a virus suspension. For competition studies in living MNs, 5.5 μg of the MAb was added to 100 μl of Neurobasal medium without phenol red (Invitrogen). For the detection of PV, a rabbit anti-PV type 1 hyperimmune serum, followed by a fluorescein isothiocyanate-conjugated goat anti-rabbit secondary antibody, was used.

Intramuscular inoculation. The precise method for intramuscular inoculation has been described previously (34). Briefly, after the mice had been anesthetized with an intraperitoneal inoculation of 300 to 400 μl of ketamine (10 mg/ml) and xylazine (0.2 mg/ml) in saline, 5 μl of PV was intramuscularly inoculated into each of four points on the left calf of each Tg mouse with a Hamilton microsyringe. A total of 20 μl of the virus suspension containing 2.7×10^7 PFU of PV was used for immunohistochemistry. In the case of inoculation with [^{35}S]methionine-labeled virus, the nerve was ligated tightly with silk thread near the junction of the thighbone and pelvis as described previously (15, 16), and 5 μl of the labeled virus was inoculated into each of four points on the left calf of each mouse. A total of 20 μl of the virus suspension contained 5×10^6 PFU (0.37 μCi).

Immunohistochemistry. The sciatic nerve was removed at a distance of ca. 2 cm from the inoculation points and was embedded. Sections, fixed with acetone-methanol (3:2) at room temperature, were reacted with rabbit hyperimmune serum against PV type 1 at 37°C for 2 h and were then treated with goat anti-rabbit IgG conjugated with fluorescein isothiocyanate at 37°C for 2 h, as previously described (34). The sections were mounted with 80% (vol/vol) glycerol and were analyzed by confocal laser scanning microscopy (Carl Zeiss MicroImaging).

Sucrose density gradient centrifugation. One and one-half hours after the intramuscular inoculation with [^{35}S]methionine-labeled PV, a portion of the sciatic nerve spanning the ligation and a point 5 mm from the site of PV injection was homogenized at 4°C in phosphate-buffered saline (8 g of NaCl, 0.2 g of KCl, 1.15 g of Na_2HPO_4, and 0.2 g of KH_2PO_4 per liter) containing 1% Nonidet P-40 and 0.1% bovine serum albumin fraction V (Sigma-Aldrich Co.). After centrifugation to remove cellular debris, the supernatant was applied to a 15-to-30% sucrose density gradient (34) and centrifuged at 39,000 rpm for 2 h at 4°C in a Beckman SW41 rotor. The radioactivity of each fraction was measured in a liquid scintillation counter.

Purification of radiolabeled PV. [^{35}S]methionine-labeled Mahoney virus was grown in HeLa S3 cells in suspension in a methionine-free medium containing [^{35}S]methionine (44). Virus in cytoplasmic extracts of infected cells was purified by using DEAE-Sepharose CL-6B (GE Healthcare Bio-Sciences KK), followed by two cycles of CsCl equilibrium centrifugation (44). The specific radioactivity of purified radiolabeled Mahoney virus was calculated to be 7.3×10^{-8} μCi/PFU.

Fluorescent labeling of PV. PV was purified by a protocol described previously (20). HeLa S3 cells were infected with Mahoney or Sabin 1 virus at a multiplicity of infection (MOI) of 10. The cells were harvested at 7 h postinfection for Mahoney virus or at 8 h postinfection for Sabin 1 virus, and the virus was purified from cytoplasmic extracts of the infected cells by using DEAE-Sepharose CL-6B, followed by sucrose density gradient and CsCl equilibrium centrifugation. Purified virus was desalted by gel filtration on a PD-10 column (GE Healthcare Bio-Sciences KK) equilibrated with PBS(−) (per liter, 8.00 g NaCl, 1.15 g Na_2HPO_4, 0.20 g KCl, 0.10 g $MgCl_2 \cdot 6H_2O$, 0.20 g KH_2PO_4 [pH 7.4]). The PV concentration was determined by measuring the absorbance at 260 nm; 1.0 optical density unit was regarded as equivalent to 9.4×10^{12} virions. Virus labeling was based on a protocol kindly provided by Lucas Pelkmans (35) and described previously (32). Briefly, PV (0.4 mg at 0.4 mg/ml) was labeled with 0.39 μl of Alexa Fluor-succinimidyl ester (10 mg/ml in dimethyl sulfoxide) according to the manufacturer's instructions (Invitrogen). The labeled virus was repurified on NAP5 columns (GE Healthcare Bio-Sciences KK), dialyzed against PBS(−), and stored at −80°C. The labeling ratio was 14 mol of dye per mol of virus. The specific infectivity of the labeled virus was not affected.

Retrograde transport assay in living cultured rodent MNs. Five or six days after being plated on glass bottom dishes (MatTek Corporation) (3, 12), spinal cord MNs were incubated with 7×10^5 PFU/well of Alexa Fluor 555-labeled strain Sabin 1 at 35.5°C or with 6×10^7 PFU/well of Alexa Fluor 488-labeled strain Mahoney at 37°C for 15 min; then they were washed and imaged by confocal laser scanning microscopy (Carl Zeiss MicroImaging). For the competition assay, MNs were incubated with or without 4.7×10^8 PFU/well of unlabeled PV or an anti-hPVR MAb at 37°C for 5 min; labeled PV and 667 μg/ml of tetramethyl rhodamine (TMR)-conjugated dextran (molecular weight, 3,000; Invitrogen) was then added, and MNs were incubated at 37°C for 15 min and then washed and observed by confocal laser scanning microscopy. Selected samples were incubated with 40 nM Alexa Fluor 555-labeled TeNT H_C (7) in complete medium for 30 min at 37°C, followed by three washes. Cells were placed in a humidified chamber maintained at 37°C, and after 20 min, images were acquired by confocal laser scanning microscopy or wide-field fluorescent microscopy using a Hamamatsu C4742-95 Orcal cooled charge-coupled device camera (Hamamatsu Photonic Systems) controlled by Kinetic Acquisition Manager 2000 software (Andor Technology).

Microinjection. MNs were injected with 0.05 mg/ml of plasmid pPVRα-GFP, encoding hPVRα-green fluorescent protein (GFP) (33), or plasmid pPVRMα-GFP, encoding a mutant form of hPVR (33), between days 5 and 6 in vitro. Eight hours after the injection, MNs were incubated with Alexa Fluor 555-labeled TeNT H_C or PV.

Tracking and data quantification. Vesicle tracking was performed on time lapse sequences as previously described (28). Speed and average speed values were determined by measuring the distance covered by each carrier between two consecutive frames and that between the initial and final tracking points, respec-

TABLE 1. PV antigen observed inside axons at 2 cm from the point of injection

Time after injection (h)	Observation of PV antigen[a] in:			
	hPVR-Tg mice		Non-Tg mice	
	Without MAb p286	With MAb p286	Without MAb p286	With MAb p286
1.5	+ − −	ND	ND	ND
3	+ + +	− − −	− − −	ND
6	+ + +	ND	± − −	ND
12	± ± −	± ± −	+ + +	ND

[a] −, PV antigen was not detected; +, PV antigen was detected in many axons; ±, PV antigen was detected in a small number of axons (each symbol stands for one sample); ND, not done.

TABLE 2. WGA antigen observed inside axons at 2 cm from the point of injection

Time after injection (h)	Observation of WGA antigen[a] in:			
	hPVR-Tg mice		Non-Tg mice	
	Without MAb p286	With MAb p286	Without MAb p286	With MAb p286
1.5	+ + ±	ND	+ + −	ND
3	+ + +	+ + ±	+ + +	+ + +
6	+ + +	+ + +	+ + +	+ + +
12	+ + ±	+ + +	+ + ±	+ + +

[a] −, PV antigen was not detected; +, PV antigen was detected in many axons; ±, PV antigen was detected in small number of axons (each symbol stands for one sample); ND, not done.

tively. Eight-bit images were assembled into Audio Video Interleave movies with Imaris (Bitplane).

RESULTS

PV shows a wide range of retrograde transport speeds in axons of hPVR-Tg mice. Previously, we reported that the in vivo transport speed of the majority of PV in hPVR-Tg mice is ca. 16 cm/day (ca. 1.9 μm/s) and comprises rates of axonal transport in the range of ca. 4 to ca. 32 cm/day (ca. 0.5 to ca. 3.7 μm/s) (34). To investigate the hPVR-independent transport of PV, the virus was coinjected with the anti-hPVR MAb p286 into the left calves of hPVR-Tg mice, and the rate of viral transport in the sciatic nerve was examined by an immunohistochemical approach (34). Transverse sections of the sciatic nerve were cut 2 cm from the injection point at various times after intramuscular inoculation with the virus and were examined for PV antigens. When 42.2 μg of MAb p286 was coinjected with the virus into hPVR-Tg mice, it took 12 h for the intramuscularly inoculated virus to reach the transection point (Table 1). This dose of MAb was sufficient to significantly diminish the incorporation of the virus into the sciatic nerve in hPVR-Tg mice (34), causing a reduction in the combined rate of PV transport, which also includes the kinetics of PV internalization, in hPVR-Tg mice to ca. 4 cm/day (ca. 0.5 μm/s). This result indicates that the slowest PV transport seen in hPVR-Tg mice in the absence of MAb p286 is likely to be hPVR independent, and the faster PV transport (more than 4 to ca. 32 cm/day; equivalent to more than 0.5 to ca. 3.7 μm/s) is likely to be hPVR dependent. Furthermore, our findings suggest that different transport mechanisms are involved in the axonal transport of intramuscularly inoculated PV in hPVR-Tg mice.

PV shows low rates of retrograde transport in the sciatic nerves of non-Tg mice. To investigate hPVR-independent PV transport, the virus was injected into the left calves of non-Tg mice and was detected by immunohistochemical analysis of transverse sections of the sciatic nerve (Table 1). The viral antigen was detected in the sciatic nerve when the sections were prepared from non-Tg mice 12 h postinjection (p.i.), whereas no axons, or only a few, showing PV antigens were detected at 6 h p.i., indicating that the rate of PV transport in non-Tg mice was ca. 4 cm/day (ca. 0.5 μm/s). These results confirm that the rate of hPVR-independent PV axonal transport is lower than that of hPVR-dependent transport in vivo. Moreover, these data show that PV is present inside axons of the sciatic nerve in non-Tg mice (data not shown).

In order to compare these transport rates with those of other molecules undergoing retrograde transport in vivo, the transport of wheat germ agglutinin (WGA) was analyzed by immunohistochemistry. WGA is a lectin that has high affinity for *N*-acetylglucosamine and *N*-acetylneuraminic acid moieties present on surface proteins (30) and is efficiently endocytosed (5, 10, 42). It has been shown that most WGA inoculated intramuscularly (into the flexor forelimb muscle) is transported retrogradely to the motor neuron cell bodies located in the ventral horn of the spinal cord in mice (4). As in the experiments described above, transverse sections of the sciatic nerve were examined for WGA antigens by immunohistochemistry (Table 2). WGA was able to reach the transection point in 1.5 h both in hPVR-Tg and in non-Tg mice and was detected at all the time points examined. These results indicate that the rate of WGA transport ranges from ca. 4 to ca. 32 cm/day (from ca. 0.5 to ca. 3.7 μm/s) and that WGA transport is independent of the presence of hPVR, as shown by the results for the MAb p286–WGA coinjection experiments reported in Table 2.

PV was incorporated into the sciatic nerves of non-Tg mice as infectious particles. We have already shown that intramuscularly inoculated PV was incorporated into the sciatic nerves of PVR-Tg21 mice as infectious particles and that the extent of incorporation was reduced by MAb p286 (34). To investigate whether PV is also incorporated into the sciatic nerves of non-Tg mice as infectious particles, [^{35}S]methionine-labeled PV was injected intramuscularly into the lower thighs of non-Tg mice, and the presence of the virus in the sciatic nerve was examined. The mice inoculated with [^{35}S]methionine-labeled virus were sacrificed at 1.5 h p.i., and the sciatic nerves were homogenized and analyzed by sucrose density gradient centrifugation as described in Materials and Methods. As shown in Fig. 1A, the majority of PV-related materials in the sciatic nerve had a sedimentation coefficient of 160S, which corresponds to the intact virion particle (2, 29). The notion that intact virion particles are transported through the axon is strengthened by our finding that a virus suspension recovered from the sciatic nerve was found to be infectious for cultured primate cells (data not shown). This 160S peak was not reduced when 42.2 μg of MAb p286 was coinjected with the virus (Fig. 1B). However, this dose of MAb was sufficient to greatly reduce the incorporation of the virus into the sciatic nerve in

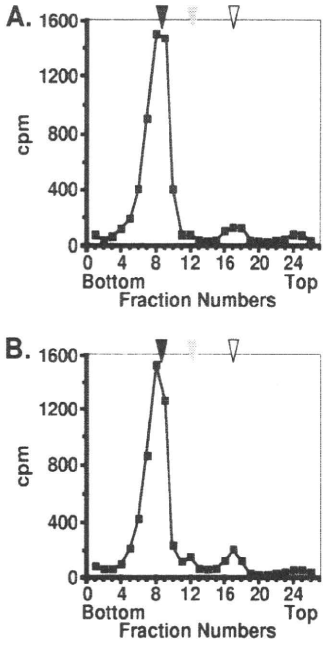

FIG. 1. Analysis of virus-related transport in the sciatic nerves of non-Tg mice. Non-Tg mice with sciatic nerve ligations were inoculated intramuscularly with 5×10^6 PFU of [^{35}S]methionine-labeled Mahoney virus, either alone (A) or mixed with the anti-hPVR MAb p286 (B). Radioactivity was recovered from the sciatic nerves and analyzed by sucrose density gradient centrifugation as described in Materials and Methods. Filled, shaded, and open arrowheads indicate 160S, 135S, and 80S, respectively.

hPVR-Tg mice (34). These results suggest that PV can be endocytosed into the neuromuscular junction (NMJ) and transported in vivo in the sciatic nerves of non-Tg mice in an hPVR-independent manner. Intramuscular inoculation of 1×10^6 PFU of the Mahoney strain did not cause neurological symptoms in non-Tg mice, although it led to the initial signs of paralysis in the inoculated limbs 48 h after injection into Tg mice (34). These data indicate that the axonal retrograde transport of PV in non-Tg mice may not result in detectable virus replication and MN death.

Axonal transport of PV in cultured rat MNs relies on hPVRs. To investigate the molecular mechanisms controlling the axonal transport of PV, we used primary MNs isolated from rat embryos. Differentiated rat pheochromocytoma (PC12) cells have been shown to internalize fluorescently labeled PV in a manner dependent on hPVRα-GFP expression (33). MNs microinjected with an hPVR-GFP-expressing plasmid were incubated with Alexa Fluor 555-labeled PV and analyzed by time lapse confocal laser scanning microscopy. hPVR-GFP is targeted to both the axonal and somatodendritic compartments in cultured rat MNs (data not shown). In these cells, fluorescently labeled PV was cotransported with hPVRα-GFP in axonal retrograde carriers (Fig. 2A; see also movie S1 in the supplemental material). In contrast, MNs not expressing hPVRα-GFP did not internalize or transport labeled PV (Fig. 2C). When unconjugated Alexa Fluor 555 was added to the cells in the same molar amount as that used for the labeled virus, no fluorescently labeled carriers were observed (data not shown). Taken together, these results demonstrate that the entry and axonal transport of PV are specific and rely totally on hPVR expression in cultured rat MNs.

For the next step, hPVRMα-GFP (33) was expressed in cultured rat MNs, and the transport of Alexa Fluor 555-labeled PV was monitored. In the hPVRMα mutant, the two basic residues of the Tctex-1 binding motif in the cytoplasmic domain of hPVRα, KXXR, were replaced by two alanines (AXXA). hPVRMα shows a lower affinity to cytoplasmic dy-

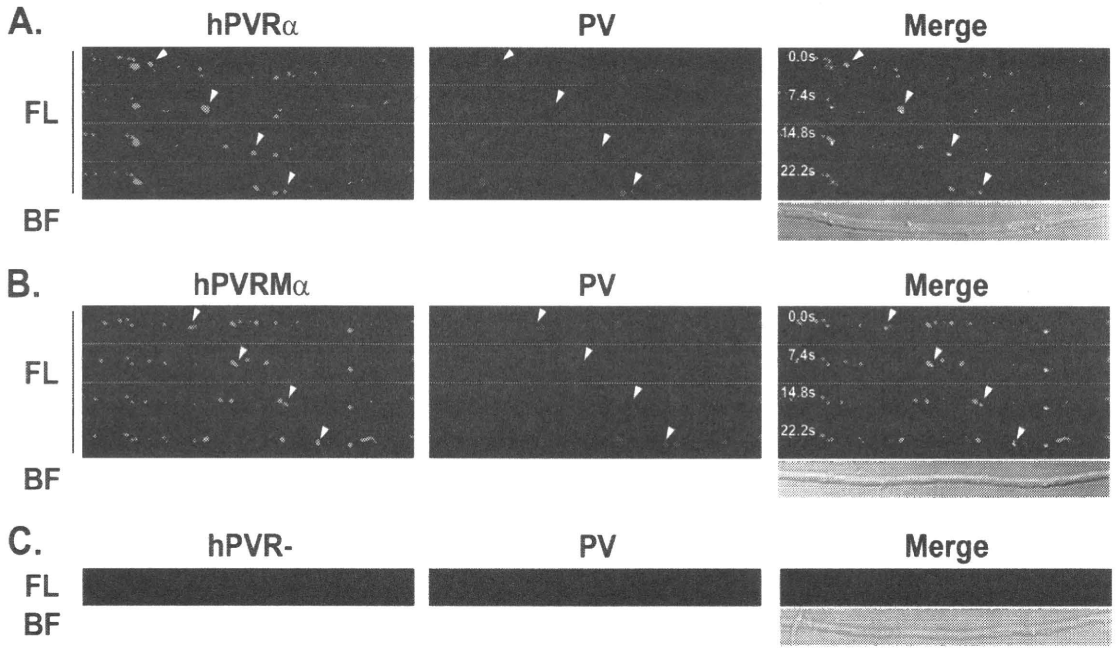

FIG. 2. Axonal transport of hPVRs and PV in cultured rat MNs. MNs expressing hPVRα-GFP (A), hPVRMα-GFP (B), or no hPVR (C) were incubated with Alexa Fluor 555-labeled PV and imaged by time lapse confocal microscopy. Carriers containing both hPVRs and PV are shown (arrowheads) in the time series provided. Green shows hPVRs, whereas red indicates the labeled PV. BF, bright-field images. The MN soma is located on the right. Bar, 10 μm.

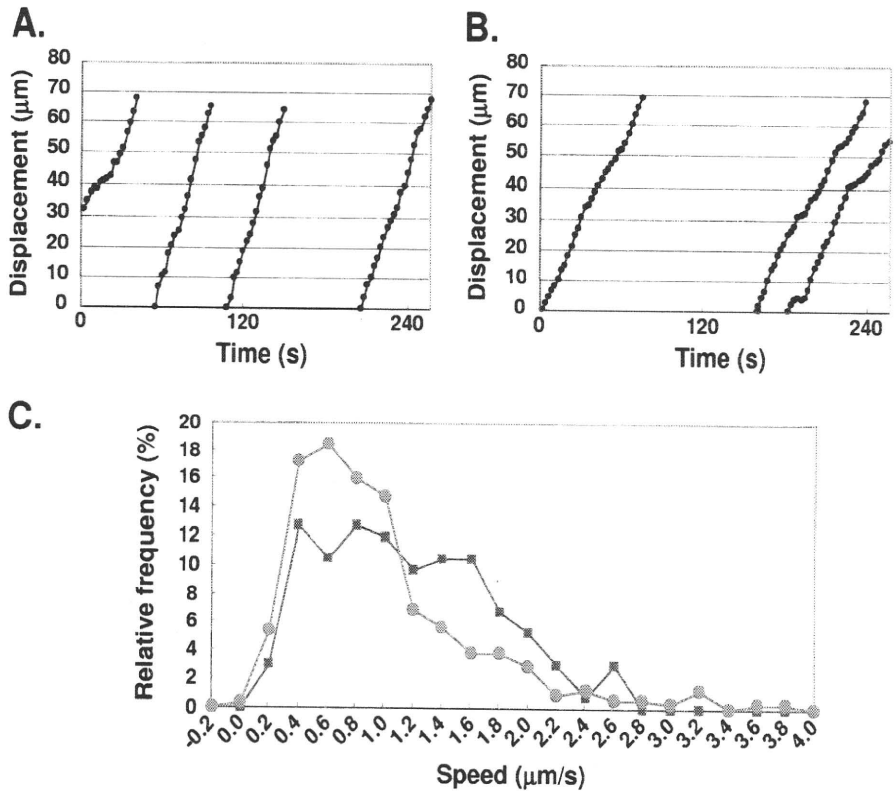

FIG. 3. Kinetic analysis of axonal transport vesicles containing both hPVRs and PV. The transport kinetics of PV were analyzed in rat MNs expressing hPVRα-GFP or hPVRMα-GFP. Only vesicles containing both hPVRs and PV were analyzed. (A and B) Representative examples of displacement graphs for vesicles containing hPVRα-GFP (A) or hPVRMα-GFP (B). (C) The speed distribution of these carriers in MNs expressing hPVRα-GFP (pink squares) or hPVRMα-GFP (green circles) is shown. The total number of movements was 134, and 22 independent carriers were observed, in two independent experiments for hPVRα-GFP. The total number of movements was 321, and 57 independent carriers were observed, in two independent experiments for hPVRMα-GFP.

nein (33) than hPVRα. Interestingly, labeled PV was retrogradely transported together with hPVRMα-GFP, as observed above for hPVRα-GFP-expressing MNs (Fig. 2B; see also movie S2 in the supplemental material). These results suggest that the axonal retrograde transport of PV in rat MNs is independent of the ability of its receptor to recruit the dynein motor complex on these axonal transport carriers.

In MNs expressing hPVRα-GFP or hPVRMα-GFP, we observed axonal vesicles containing hPVRs that did not carry PV even after preincubation of labeled PV with MNs. Interestingly, these organelles displayed bidirectional transport (data not shown), strongly suggesting that in rat MNs, the directionality of the carriers containing only hPVRs differ from that of those containing both hPVRs and its ligand. It is possible that vesicles containing only hPVR carry newly synthesized hPVR along the secretory pathway or that they represent endosomes internalized prior to, or independently of, PV addition. As shown in Fig. 2C, we were not able to observe any PV-positive endosome lacking hPVRs. This observation indicates that PV is transported together with hPVR in cultured rat MNs.

Expression of hPVRMα-GFP impairs fast retrograde transport in rat MNs. To assess whether rat MNs in culture expressing hPVRα-GFP or hPVRMα-GFP show identical axonal transport characteristics, we examined the kinetics of PV transport under these conditions. As shown in Fig. 3, the transport kinetics were reproducibly different. Displacement graphs of representative examples of the carriers are shown in Fig. 3A and B. In cells expressing hPVRα-GFP, two speed components that differ in their average transport velocity were estimated. The fast speed component was ≥1.4 μm/s, whereas the slow component was centered between 0.4 μm/s and 1.0 μm/s (Fig. 3C). In MNs expressing hPVRMα-GFP, the relative frequency of the fast speed component was greatly reduced, while that of the slow speed component was increased compared to those observed in MNs expressing hPVRα-GFP. These results suggest that the high-affinity interaction of hPVR with cytoplasmic dynein is required to ensure fast retrograde transport of axonal carriers containing both hPVR and PV in cultured rat MNs.

TeNT H_C and hPVRs share retrograde transport carriers in rat MNs. To correlate the axonal transport features of hPVR with an established retrograde transport cargo in rat MNs, we compared the dynamics of hPVRα-GFP and hPVRMα-GFP with that of the fluorescently labeled binding fragment of tetanus toxin (TeNT H_C). TeNT H_C enters the nervous system at the NMJ, where it is internalized and retrogradely transported along the MN axons, following a pathway shared with neurotrophins and their receptors (7). Rat MNs were incubated with TeNT H_C and, after washing, were directly imaged. As reported previously, TeNT H_C underwent fast retrograde axonal transport following established kinetics (Fig. 4). Interestingly, in MNs expressing hPVRα-GFP, both hPVRα-GFP and TeNT H_C colocalized in axonal carriers that were transported retrogradely (data not shown). Similarly, simultaneous transport of hPVRMα-GFP and TeNT H_C was observed (data not shown).

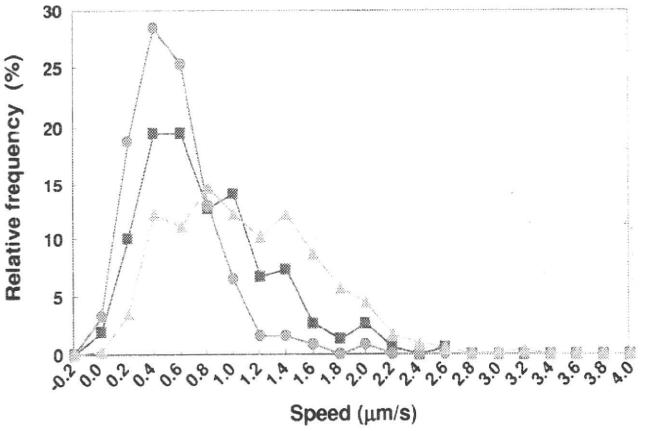

FIG. 4. Kinetic analysis of axonal transport vesicles containing both hPVRs and TeNT H_C. Shown are speed distribution profiles of carriers containing TeNT H_C in control rat MNs (orange triangles) or MNs expressing hPVRα-GFP (pink squares) or hPVRMα-GFP (green circles). Only vesicles containing both hPVRs and TeNT H_C were analyzed in MNs expressing hPVRs. For the control, the total number of movements was 482, and 78 independent carriers were observed; for hPVRα-GFP, the total number of movements was 149, and 38 independent carriers were observed; for hPVRMα-GFP, the total number of movements was 123, and 33 independent carriers were observed.

These results suggest that hPVRs are cotransported in axonal carriers containing not only PV but also TeNT H_C. With regard to the transport kinetics, the speed distribution profile of carriers containing both hPVRα-GFP and TeNT H_C was not dramatically different from that of organelles containing TeNT H_C alone in terms of the positions of the average speed components, although the slower component was slightly increased in hPVRα-GFP-containing carriers (Fig. 4). In contrast, carriers containing both hPVRMα-GFP and TeNT H_C (Fig. 4) displayed much slower kinetics than hPVRα-GFP-containing organelles, with the slower speed component contributing to the majority of the speed profile of these organelles (Fig. 4). These results suggest that expression in rat MNs of an hPVR mutant with an impaired Tctex-1 binding site influences the transport kinetics of TeNT H_C in this system similarly to that of PV. These findings indicate that hPVR plays a functional role in the traffic of TeNT H_C-positive carriers, and they raise the possibility that hPVR is a main dynein-interacting protein with a primary role in axonal retrograde transport.

Axonal retrograde transport of PV is dependent on hPVR in hPVR-Tg mice. To assess whether PV can be transported in isolated MNs of hPVR-Tg mice, the transport of a fluorescently labeled virus was tested in MNs isolated from this mouse strain. Alexa Fluor 488-labeled PV was added to hPVR-Tg mouse-derived MNs in culture and was imaged by confocal laser scanning microscopy. As previously observed in rat MNs expressing hPVRα-GFP, the untagged hPVR showed a nonpolarized distribution in spinal MNs isolated from hPVR-Tg mice (data not shown). As expected, fluorescent PV was retrogradely transported in the axons of these MNs in culture. This result indicates that the axonal transport pathway for PV observed in hPVR-Tg mice is preserved in isolated MNs. When Alexa Fluor 488-labeled PV was added to spinal MNs isolated from hPVR-Tg mice together with fluorescent dextran (TMR-dextran) as a fluid-phase endosomal marker, distinct populations of vesicles were observed. Whereas one of these vesicle pools contained both fluorescently labeled PV and TMR-dextran (Fig. 5A; see also movie S3 in the supplemental material), a second class of vesicles labeled by fluorescently labeled PV contained undetectable levels of dextran (Fig. 5B; see also movie S4 in the supplemental material). Both types of PV-containing axonal carriers undergo retrograde transport (Fig. 5). These results are in agreement with the PV transport characteristics observed in differentiated PC12 cells (33) and suggest that PV and dextran are incorporated into the same vesicles and cotransported retrogradely in cultured MNs of hPVR-Tg mice. As expected, vesicles containing TMR-conjugated dextran with undetectable or insignificant amounts of labeled PV were also present. Interestingly, these vesicles undergo bidirectional transport (data not shown). The number of carriers for each vesicle pool was as follows: 45 carriers containing both fluorescent PV and dextran, 19 carriers containing PV with undetectable amounts of dextran, and 28 organelles containing dextran with undetectable or insignificant amounts of PV (92 carriers in total in two independent experiments). From these observations, some vesicles containing only fluorescently labeled PV or only TMR-conjugated dextran might exist in cultured MNs.

To investigate the specificity of transport of the labeled virus, competition experiments with unlabeled PV were performed. The transport of Alexa Fluor 488-labeled PV strain Mahoney and TMR-conjugated dextran was assessed in MNs derived from hPVR-Tg mice upon incubation with 4.7×10^8 PFU of unlabeled PV strain Mahoney (Fig. 5C). In contrast with the results obtained in the absence of unlabeled PV (Fig. 5A), no transport of labeled PV was detected under these conditions, whereas the transport of TMR-conjugated dextran was unmodified (Fig. 5C; see also movie S5 in the supplemental material). Furthermore, the transport of Alexa Fluor 488-labeled PV, but not that of TMR-conjugated dextran, was blocked by the addition of an anti-hPVR MAb to MNs isolated from hPVR-Tg mice (Fig. 5D; see also movie S6 in the supplemental material). These results indicate that the axonal transport of the fluorescently labeled virus in cultured MNs derived from hPVR-Tg mice is specific and is strictly hPVR dependent.

DISCUSSION

In this study, we employed murine and rat MNs in culture as well as intact sciatic nerves in situ to provide insights into the mechanisms of uptake and axonal retrograde transport of PV. Differentiated MNs in culture are considered to reflect the native characteristics of MNs in vivo. We have recently developed a method to fluorescently label PV virions without altering their biological properties (32). In addition, microinjected hPVR-GFP was successfully expressed in rat MNs. These techniques allowed us to observe fluorescently labeled PV and hPVR-GFP in living MNs and to analyze the characteristics of the axonal retrograde transport of PV.

Using differentiated PC12 cells, we previously showed that hPVRMα vesicles loaded with PV move bidirectionally, whereas PV-containing hPVRα carriers move strictly retrogradely (33). These data do not overlap with the transport kinetics of hPVRMα- and hPVRα-containing vesicles ob-

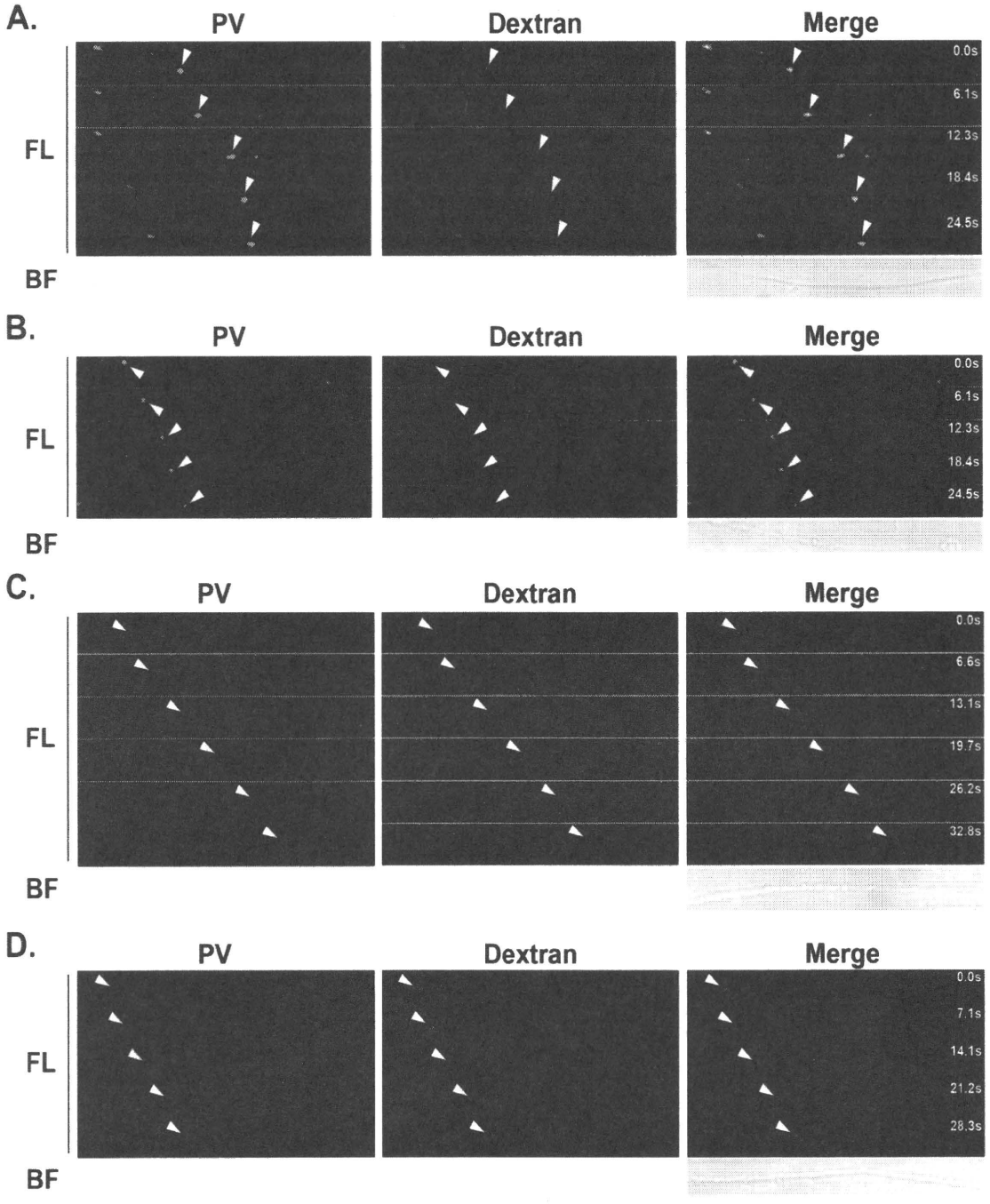

FIG. 5. The transport mechanism of PV in isolated MNs derived from hPVR-Tg mice is hPVR specific. (A) Axonal carriers containing both PV and dextran are retrogradely transported in MNs isolated from hPVR-Tg mice. MNs derived from hPVR-Tg mice were incubated with Alexa Fluor 488-labeled PV and TMR-conjugated dextran, and their axonal transport was imaged as described in Materials and Methods (arrowheads). (B) Vesicles containing PV and undetectable levels of dextran were also retrogradely transported in cultured MNs of hPVR-Tg mice (arrowheads). (C) Axonal transport of Alexa Fluor 488-labeled PV was not observed in the presence of unlabeled PV. MNs isolated from hPVR-Tg mice were incubated with Alexa Fluor 488-labeled PV and TMR-conjugated dextran in the presence of unlabeled PV prior to imaging. Arrowheads indicate PV-negative, TMR-positive transported organelles. (D) Axonal transport of Alexa Fluor 488-labeled PV was not observed in the presence of an anti-hPVR MAb. MNs isolated from hPVR-Tg mice were incubated with Alexa Fluor 488-labeled PV and TMR-conjugated dextran in the presence of an anti-hPVR MAb prior to imaging. Arrowheads indicate PV-negative, TMR-positive transported organelles. PV appears green, while dextran appears red. The rightmost panels are the merged images. Cell bodies are located on the right. Bar, 10 μm.

served in rat MNs in this study. This discrepancy might be due to differences in the cells analyzed, as, for example, with the mixed polarity seen in PC12 neurites. MNs in culture are considered to be superior to differentiated PC12 cells in reflecting the original characteristics of MNs in vivo.

Our results with MNs isolated from hPVR-Tg mice show that some vesicles containing only fluorescently labeled PV or only TMR-conjugated dextran might exist in cultured MNs. It is possible that TMR-conjugated dextran can be sorted into different vesicles from labeled PV after the endocytosis in cultured MNs. It is also possible that the vesicle is so small as to allow very little TMR-conjugated dextran in the residual luminal space.

Based on our previous report, the velocity of PV transport in hPVR-Tg mice ranges from ca. 4 to ca. 32 cm/day (from ca. 0.5 to ca. 3.7 μm/s) (34). This closely matches the rate observed in this work for hPVR-dependent PV transport. In contrast, the rates of hPVR-independent uptake and transport of PV in non-Tg mice, and in hPVR-Tg mice in the presence of MAb p286, are comparable to each other and much lower (ca. 4 cm/day; equivalent to ca. 0.5 μm/s). WGA was transported in hPVR-Tg or non-Tg mice at rates ranging from ca. 0.5 to ca. 3.7 μm/s, similar to those of hPVR-dependent PV transport. These results strongly suggest that different systems for PV transport do coexist in the axons of hPVR-Tg mice. In sharp contrast, no hPVR-independent PV transport was observed in cultured MNs under our experimental conditions. Although the reason is presently unknown, this discrepancy may derive from the different conditions occurring in vivo and in primary MNs in culture. At present, we cannot estimate with sufficient precision the MOI for intramuscular inoculation with PV. The actual MOI in vivo might be much higher than that in primary culture because of the anatomical structure of the NMJ, resulting in a high yield of hPVR-independent incorporation of PV in vivo. Alternatively, a still unidentified PV receptor may be expressed at NMJs in vivo, causing a delay in PV uptake or its targeting to an alternative endocytic route engaged only upon stimulation, a condition not investigated in isolated MNs.

TeNT H_C was transported at rates as high as 3.6 μm/s in cultured MNs expressing hPVRα or hPVRMα, and its speed distribution curves (Fig. 4 and data not shown) fit well with those previously reported (3). Interestingly, the highest rate of TeNT transport has been shown to be 7.5 mm/h (ca. 2.1 μm/s) in vivo (41). According to these results, the rate of TeNT transport in isolated rat MNs correlates well with that observed in vivo. The fastest component of PV transport in cultured rat MNs expressing hPVRα-GFP was ca. 2.6 μm/s, although it is a small population. The rate of the PV transport observed in the cultured MNs may correlate with the hPVR-dependent PV velocity in vivo (>0.5 to ca. 3.7 μm/s). The rate of the slow component of the hPVR-independent PV transport seen in vivo (ca. 1.7 mm/h; ca. 0.5 μm/s) (Fig. 6Ac and Bc) is similar to that of the slow component seen in cultured MNs (0.5 μm/s) (Fig. 6Cb). This agreement seems to be a coincidence, since it is unlikely that the mechanisms for hPVR-dependent and hPVR-independent transport are identical. However, it might be possible that the slow component in cultured MNs requires hPVR during endocytosis, whereas its transport may be hPVR independent (Fig. 6Cb). In the presence of an anti-hPVR MAb in hPVR-Tg mice, hPVR-independent transport of PV was observed. Based on this observation, it is therefore possible that similar hPVR-independent transport occurs in hPVR-Tg mice even in the absence of the anti-hPVR MAb and that some of the PV-containing vesicles in hPVR-Tg mice exhibit hPVR-independent slow transport (Fig. 6Ab).

It has been reported that the rate of transport of horseradish peroxidase-conjugated WGA in hamster facial MNs distributes continuously from 1.0 to 1.4 mm/h (0.3 to 0.4 μm/s) to 8.3 to 10.9 mm/h (2.3 to 3.0 μm/s) (19). Although the probes used in this study are different, the rate of WGA transport we observed in the sciatic nerve (from ca. 0.5 to 3.7 μm/s) seems appropriate. It has been reported that retrograde transport of WGA exhibits biphasic kinetics in pike olfactory nerve c-fibers (6).

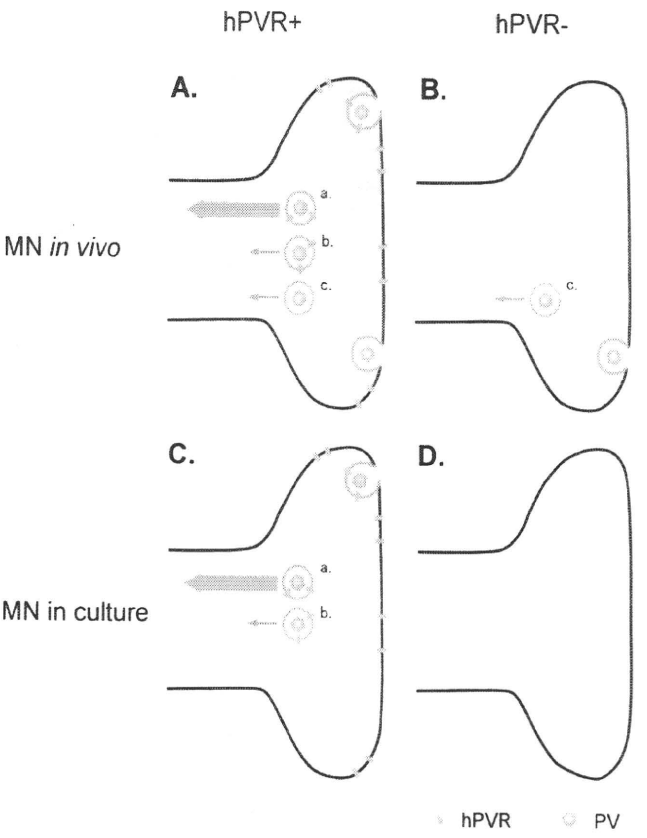

FIG. 6. Mechanisms for hPVR-dependent and -independent transport of PV in MNs. (A) In hPVR-Tg mice, PV is endocytosed after binding to hPVR (in green). Most of the hPVR-containing vesicles are retrogradely transported in an hPVR-dependent manner (orange membrane carrier). The transport of these vesicles shows fast kinetics. In vivo, hPVR-independent endocytosis and transport of PV also occur (purple membrane organelle), possibly mediated by a still unidentified PV receptor expressed at NMJs. Alternatively, hPVR-independent endocytosis may be promoted by synaptic activity, which occurs in vivo but was not tested in isolated MNs. PV-containing vesicles with or without hPVR can be retrogradely transported in an hPVR-independent manner with slow kinetics. (B) In non-Tg mice, PV is endocytosed and transported with slow kinetics in an hPVR-independent manner. (C) In isolated MNs, only hPVR-dependent PV endocytosis is detected. The hPVR-dependent transport of axonal carriers shows fast kinetics. It might be possible that the slow component in cultured MNs requires hPVR during endocytosis, whereas its transport may be hPVR independent. (D) No endocytosis of PV is detected in control cultured MNs lacking hPVR. The green solid arrows denote hPVR-dependent fast retrograde transport (Aa and Ca), whereas the orange arrows indicate slow retrograde transport (Ab, Ac, Bc, and Cb).

Nevertheless, the biphasic peaks overlapped with each other, and the rate of the WGA transport distributed continuously. Since WGA binds glycoproteins ubiquitously distributed on the cell surface, it is likely that WGA is transported by multiple classes of axonal organelles with overlapping kinetic properties. Compared with WGA-positive carriers, the hPVR-independent transport of PV exhibited only slow kinetics. This result strengthens the possibility that the hPVR-independent uptake of PV at the NMJ is specific and that the unknown PV receptor mentioned above is involved in the hPVR-independent transport of PV in vivo.

Lalli et al. reported a dramatic decrease in the fast (1.15-μm/s) speed component of TeNT H_C transport in MNs treated with the cytoplasmic dynein inhibitor *erythro*-9-[3-2-(hy-

droxynonyl)] adenine (EHNA) (36, 38), whereas the intermediate (0.53-μm/s) component was unaffected (27). Similarly, we have observed a decrease in the fast component (≥1.4 μm/s) of PV transport in cultured MNs expressing hPVRMα, which has a reduced affinity with the dynein complex. Taken together, these findings suggest that the high affinity of hPVR with cytoplasmic dynein contributes to the fast component of the axonal retrograde transport of PV in cultured MNs. Although it does not bind PV, the murine homologue of hPVR may play an indirect role in axonal transport of the virus in non-Tg mice, for example, by associating with hPVRMα, by competing for dynein recruitment or influencing its endosomal sorting. In this regard, the loss-of-function phenotype for PV transport observed for hPVRMα may be enhanced by performing these experiments in a murine homologue of an hPVR-null background.

Residual low levels of PV transport may be present in isolated MNs not expressing hPVR, but they may be undetectable by our experimental system. A possible explanation is that the individual PV virions may be less concentrated in axons lacking hPVR and thus less likely to be observed by direct fluorescence. This seems unlikely, however, given the rather high ratio of incorporation of Alexa Fluor dye into the fluorescent PV (14 mol of dye per mol of virus; see Materials and Methods). Another possibility is that the hPVR-independent route of PV uptake and transport is much less efficient than the hPVR-dependent route, resulting in a very low frequency of transport events in isolated MNs.

ACKNOWLEDGMENTS

We thank A. Ohmura for breeding the mice and E. Suzuki for help in the preparation of the manuscript.

This work was supported in part by Grants-in-Aid for Advanced Medical Science Research by the Ministry of Education, Culture, Sports, Science, and Technology (MEXT); a Grant-in-Aid for Scientific Research on Priority Areas; a Grant-in-Aid for Scientific Research (S); a Grant-in-Aid for Young Scientists (B); Human Frontier Science Program, Special Coordination Funds for Promoting Science and Technology; a contracted research allowance, "Research and Development in a New Converting Field Based on Nanotechnology and Materials Science," from MEXT; the Industrial Technology Research Grant Program in 2002 from the New Energy and Industrial Technology Development Organization (NEDO) of Japan; The Naito Foundation; a grant from the Ministry of Health, Labor and Welfare of Japan; and Cancer Research UK.

REFERENCES

1. **Aniento, F., N. Emans, G. Griffiths, and J. Gruenberg.** 1993. Cytoplasmic dynein-dependent vesicular transport from early to late endosomes. J. Cell Biol. **123:**1373–1387.
2. **Arita, M., S. Koike, J. Aoki, H. Horie, and A. Nomoto.** 1998. Interaction of poliovirus with its purified receptor and conformational alteration in the virion. J. Virol. **72:**3578–3586.
3. **Bohnert, S., and G. Schiavo.** 2005. Tetanus toxin is transported in a novel neuronal compartment characterized by a specialized pH regulation. J. Biol. Chem. **280:**42336–42344.
4. **Borges, L. F., and R. L. Sidman.** 1982. Axonal transport of lectins in the peripheral nervous system. J. Neurosci. **2:**647–653.
5. **Broadwell, R. D., and B. J. Balin.** 1985. Endocytic and exocytic pathways of the neuronal secretory process and trans-synaptic transfer of wheat germ agglutinin-horseradish peroxidase in vivo. J. Comp. Neurol. **242:**632–650.
6. **Buchner, K., D. Seitz-Tutter, K. Schonitzer, and D. G. Weiss.** 1987. A quantitative study of anterograde and retrograde axonal transport of exogenous proteins in olfactory nerve C-fibers. Neuroscience **22:**697–707.
7. **Deinhardt, K., O. Berninghausen, H. J. Willison, C. R. Hopkins, and G. Schiavo.** 2006. Tetanus toxin is internalized by a sequential clathrin-dependent mechanism initiated within lipid microdomains and independent of epsin1. J. Cell Biol. **174:**459–471.
8. **Driskell, O. J., A. Mironov, V. J. Allan, and P. G. Woodman.** 2007. Dynein is required for receptor sorting and the morphogenesis of early endosomes. Nat. Cell Biol. **9:**113–120.
9. **Freistadt, M. S., and V. R. Racaniello.** 1991. Mutational analysis of the cellular receptor for poliovirus. J. Virol. **65:**3873–3876.
10. **Gonatas, N. K., C. Harper, T. Mizutani, and J. O. Gonatas.** 1979. Superior sensitivity of conjugates of horseradish peroxidase with wheat germ agglutinin for studies of retrograde axonal transport. J. Histochem. Cytochem. **27:**728–734.
11. **Gromeier, M., and E. Wimmer.** 1998. Mechanism of injury-provoked poliomyelitis. J. Virol. **72:**5056–5060.
12. **Henderson, C. E.** 1995. Neurotrophic factors as therapeutic agents in amyotrophic lateral sclerosis. Potential and pitfalls. Adv. Neurol. **68:**235–240.
13. **Hirokawa, N.** 1998. Kinesin and dynein superfamily proteins and the mechanism of organelle transport. Science **279:**519–526.
14. **Hirokawa, N., Y. Noda, and Y. Okada.** 1998. Kinesin and dynein superfamily proteins in organelle transport and cell division. Curr. Opin. Cell Biol. **10:**60–73.
15. **Hirokawa, N., R. Sato-Yoshitake, N. Kobayashi, K. K. Pfister, G. S. Bloom, and S. T. Brady.** 1991. Kinesin associates with anterogradely transported membranous organelles in vivo. J. Cell Biol. **114:**295–302.
16. **Hirokawa, N., R. Sato-Yoshitake, T. Yoshida, and T. Kawashima.** 1990. Brain dynein (MAP1C) localizes on both anterogradely and retrogradely transported membranous organelles in vivo. J. Cell Biol. **111:**1027–1037.
17. **Holzbaur, E. L., and R. B. Vallee.** 1994. Dyneins: molecular structure and cellular function. Annu. Rev. Cell Biol. **10:**339–372.
18. **Howe, H., and D. Bodian.** 1942. Neural mechanisms in poliomyelitis. Commonwealth Fund, New York, NY.
19. **Huppenbauer, C. B., L. Tanzer, and K. J. Jones.** 2001. Detection of retrogradely transported WGA-HRP in axotomized adult hamster facial motoneurons occurs after initiation of the axon reaction. J. Neurocytol. **30:**907–916.
20. **Kajigaya, S., H. Arakawa, S. Kuge, T. Koi, N. Imura, and A. Nomoto.** 1985. Isolation and characterization of defective-interfering particles of poliovirus Sabin 1 strain. Virology **142:**307–316.
21. **King, S. M., J. F. Dillman III, S. E. Benashski, R. J. Lye, R. S. Patel-King, and K. K. Pfister.** 1996. The mouse t-complex-encoded protein Tctex-1 is a light chain of brain cytoplasmic dynein. J. Biol. Chem. **271:**32281–32287.
22. **Kohara, M., S. Abe, T. Komatsu, K. Tago, M. Arita, and A. Nomoto.** 1988. A recombinant virus between the Sabin 1 and Sabin 3 vaccine strains of poliovirus as a possible candidate for a new type 3 poliovirus live vaccine strain. J. Virol. **62:**2828–2835.
23. **Koike, S., H. Horie, I. Ise, A. Okitsu, M. Yoshida, N. Iizuka, K. Takeuchi, T. Takegami, and A. Nomoto.** 1990. The poliovirus receptor protein is produced both as membrane-bound and secreted forms. EMBO J. **9:**3217–3224.
24. **Koike, S., I. Ise, and A. Nomoto.** 1991. Functional domains of the poliovirus receptor. Proc. Natl. Acad. Sci. USA **88:**4104–4108.
25. **Koike, S., C. Taya, J. Aoki, Y. Matsuda, I. Ise, H. Takeda, T. Matsuzaki, H. Amanuma, H. Yonekawa, and A. Nomoto.** 1994. Characterization of three different transgenic mouse lines that carry human poliovirus receptor gene—influence of the transgene expression on pathogenesis. Arch. Virol. **139:**351–363.
26. **Koike, S., C. Taya, T. Kurata, S. Abe, I. Ise, H. Yonekawa, and A. Nomoto.** 1991. Transgenic mice susceptible to poliovirus. Proc. Natl. Acad. Sci. USA **88:**951–955.
27. **Lalli, G., S. Gschmeissner, and G. Schiavo.** 2003. Myosin Va and microtubule-based motors are required for fast axonal retrograde transport of tetanus toxin in motor neurons. J. Cell Sci. **116:**4639–4650.
28. **Lalli, G., and G. Schiavo.** 2002. Analysis of retrograde transport in motor neurons reveals common endocytic carriers for tetanus toxin and neurotrophin receptor p75NTR. J. Cell Biol. **156:**233–239.
29. **Lonberg-Holm, K., L. B. Gosser, and J. C. Kauer.** 1975. Early alteration of poliovirus in infected cells and its specific inhibition. J. Gen. Virol. **27:**329–342.
30. **Månsson, J., and S. Olofsson.** 1983. Binding specificities of the lectins from *Helix pomatia*, soybean and peanut against different glycosphingolipids in liposome membranes. FEBS Lett. **156:**249–252.
31. **Nathanson, N., and A. D. Langmuir.** 1963. The Cutter incident: poliomyelitis following formaldehyde-inactivated poliovirus vaccination in the United States during the spring of 1955. III. Comparison of the clinical character of vaccinated and contact cases occurring after use of high rate lots of Cutter vaccine. Am. J. Hyg. **78:**61–81.
32. **Ohka, S., H. Igarashi, N. Nagata, M. Sakai, S. Koike, T. Nochi, H. Kiyono, and A. Nomoto.** 2007. Establishment of a poliovirus oral infection system in human poliovirus receptor-expressing transgenic mice that are deficient in alpha/beta interferon receptor. J. Virol. **81:**7902–7912.
33. **Ohka, S., N. Matsuda, K. Tohyama, T. Oda, M. Morikawa, S. Kuge, and A. Nomoto.** 2004. Receptor (CD155)-dependent endocytosis of poliovirus and retrograde axonal transport of the endosome. J. Virol. **78:**7186–7198.
34. **Ohka, S., W. X. Yang, E. Terada, K. Iwasaki, and A. Nomoto.** 1998. Retrograde transport of intact poliovirus through the axon via the fast transport system. Virology **250:**67–75.

35. **Pelkmans, L., J. Kartenbeck, and A. Helenius.** 2001. Caveolar endocytosis of simian virus 40 reveals a new two-step vesicular-transport pathway to the ER. Nat. Cell Biol. **3**:473–483.
36. **Penningroth, S. M., A. Cheung, P. Bouchard, C. Gagnon, and C. W. Bardin.** 1982. Dynein ATPase is inhibited selectively in vitro by *erythro*-9-[3-2-(hydroxynonyl)]adenine. Biochem. Biophys. Res. Commun. **104**:234–240.
37. **Ren, R., and V. R. Racaniello.** 1992. Poliovirus spreads from muscle to the central nervous system by neural pathways. J. Infect. Dis. **166**:747–752.
38. **Reynolds, A. J., S. E. Bartlett, and I. A. Hendry.** 1998. Signalling events regulating the retrograde axonal transport of 125I-beta nerve growth factor in vivo. Brain Res. **798**:67–74.
39. **Selinka, H. C., A. Zibert, and E. Wimmer.** 1991. Poliovirus can enter and infect mammalian cells by way of an intercellular adhesion molecule 1 pathway. Proc. Natl. Acad. Sci. USA **88**:3598–3602.
40. **Shiroki, K., T. Ishii, T. Aoki, M. Kobashi, S. Ohka, and A. Nomoto.** 1995. A new *cis*-acting element for RNA replication within the 5′ noncoding region of poliovirus type 1 RNA. J. Virol. **69**:6825–6832.
41. **Stöckel, K., M. Schwab, and H. Thoenen.** 1975. Comparison between the retrograde axonal transport of nerve growth factor and tetanus toxin in motor, sensory and adrenergic neurons. Brain Res. **99**:1–16.
42. **Trojanowski, J. Q., J. O. Gonatas, and N. K. Gonatas.** 1981. Conjugates of horseradish peroxidase (HRP) with cholera toxin and wheat germ agglutinin are superior to free HRP as orthogradely transported markers. Brain Res. **223**:381–385.
43. **Vallee, R. B., and M. P. Sheetz.** 1996. Targeting of motor proteins. Science **271**:1539–1544.
44. **Yang, W. X., T. Terasaki, K. Shiroki, S. Ohka, J. Aoki, S. Tanabe, T. Nomura, E. Terada, Y. Sugiyama, and A. Nomoto.** 1997. Efficient delivery of circulating poliovirus to the central nervous system independently of poliovirus receptor. Virology **229**:421–428.

The Picornaviruses
Edited by Ellie Ehrenfeld, Esteban Domingo, and Raymond P. Roos

Chapter 21

Poliomyelitis

SATOSHI KOIKE AND AKIO NOMOTO

INTRODUCTION

Poliovirus (PV) is the causative agent of poliomyelitis, an acute human disease of the central nervous system (CNS). PV pathogenesis was initially studied in nonhuman primates, beginning soon after the virus was isolated by Landsteiner and Popper (62). General outlines of the sequential events in PV infection were delineated by Bodian, Sabin, and others in the 1950s (6, 8, 106; recently reviewed in references 73, 76, 85, and 99) (Fig. 1).

In humans, PV is ingested and multiplies in the oropharyngeal and intestinal mucosa. Infected humans shed virus in pharyngeal secretions and feces for several weeks, allowing for transmission of the virus. The virus spreads to the draining lymph nodes, where it replicates further, and then spreads via the efferent lymphatic vessels and thoracic duct to enter the bloodstream. Viremia is established, resulting in exposure of almost all tissues to virus. PV replication occurs in extraneural tissues such as spleen, liver, pancreas, muscle, and adipose tissue; however, the amount of recovered virus is low and prominent pathological lesions are not observed in these tissues. Viremia continues for approximately a week, until neutralizing antibodies appear in the blood. Most natural infections of humans end at this stage with a minor illness, such as fever, sore throat, and intestinal upset, a course commonly followed with other enterovirus infections.

In less than 1% of individuals infected with wild-type (wt) PV, the virus spreads to the CNS, where it replicates efficiently. Therefore, neurological disease caused by PV is considered an accidental phenomenon accompanying the common enteric infection. PV replicates in restricted sites of the CNS, including motor neurons in the spinal cord (which leads to flaccid paralysis), the brain stem, and cortex.

Since the development of effective PV vaccines (104, 105, 107), studies on PV pathogenesis using nonhuman primate models have become less common. In 1990, the development of a transgenic (tg) mouse model provided new approaches for the study of PV infection (57, 102). The tg model has provided an opportunity to study the reasons that PV fails to reach the final target tissues in most cases of infection. This failure suggests that there are barriers that prevent the progression and dissemination of PV infection and that neurological disease only occurs when virus succeeds in traveling across the barriers. One may consider that each step of PV infection is a combat between the virus and a host barrier. The nature of some of these barriers has been clarified using the tg mouse model. This chapter will provide a review of recent advances in our understanding of PV pathogenicity from this perspective.

SPECIES SPECIFICITY OF PV INFECTION: THE HOST RANGE BARRIER

PV Receptor and Host Range

The host range of most PV strains is restricted to primates (reviewed in reference 40), with humans as the natural host. Old World monkeys are susceptible to experimental infection, while the susceptibility of New World monkeys is irregular and only some species are susceptible to only some PV strains. Prosimians and nonprimate species are generally not susceptible to PV except for adapted PV strains (2). This host range restriction is determined by the ability of virus to bind to a cell surface receptor, the PV receptor (PVR) (45).

The PVR was identified by taking advantage of the species-specific nature of infection. Mouse cells are not susceptible to PV infection but permit PV

Satoshi Koike • Neurovirology Project, Tokyo Metropolitan Institute of Medical Science, Tokyo Metropolitan Organization for Medical Research, 2-1-6 Kamikitazawa, Setagaya-ku, Tokyo 156-8506, Japan. **Akio Nomoto** • Institute of Microbial Chemistry, 3-14-23 Kamiosaki, Shinagawa-ku, Tokyo 141-0021, Japan.

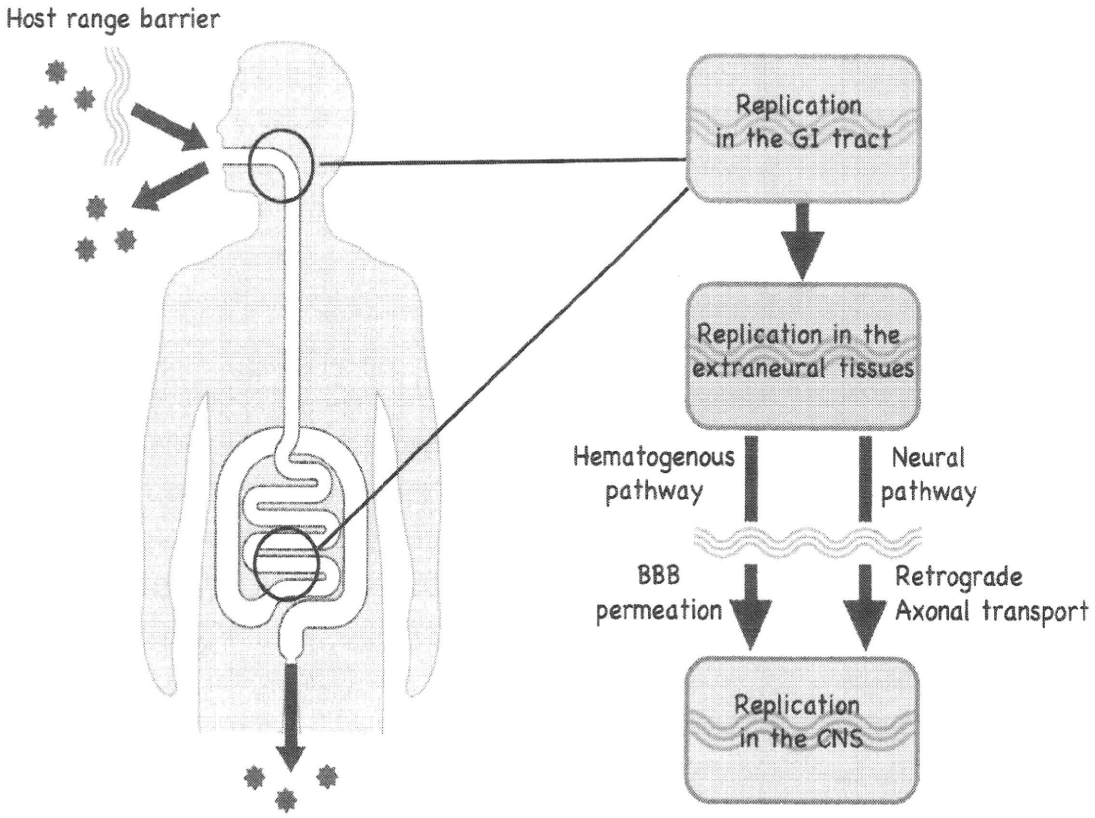

Figure 1. Scheme of PV pathogenesis and possible barriers that prevent PV dissemination. There are several host barriers that block the progression of PV dissemination. The host range of PV is restricted to simians, so other animal species are not susceptible to PV infection (host range barrier). In humans, after PV is ingested, PV initially replicates in the oropharyngeal and intestinal mucosa and enters the host despite a physical barrier at the GI mucosa (GI tract barriers). When PV reaches the blood, PV replicates poorly in the extraneural tissues, suggesting the presence of a barrier that prevents efficient replication of PV in these tissues. The CNS is physically isolated from the extraneural tissues by the blood-brain barrier (BBB), which acts as a physical barrier preventing free movement of substances between the bloodstream and the parenchyma of the CNS. PV permeates this barrier by an unknown mechanism. PV also reaches the CNS via retrograde axonal transport, a pathway for PV that is dependent on the PVR. PV finally replicates in neurons in the CNS. The replication sites in the CNS are restricted to certain neurons, suggesting the presence of unknown barriers in nonsusceptible neurons. Replication of attenuated PV strains is strongly suppressed in neurons, suggesting PV strain-specific barriers in the CNS.

replication when PV RNA is transfected, circumventing infection through the cell surface (36–38). Miller et al. (69) found that human-mouse hybrid cells carrying human chromosome 19 were susceptible to PV. A monoclonal antibody directed against the cell surface of HeLa cells, D171, was able to block PV infection (80). D171 also bound to hybrid cells carrying human chromosome 19. In order to identify the PV receptor, Mendelsohn et al. (67) transformed mouse cells that were not susceptible to PV to susceptible cells through the transfer of human genomic DNA. The *PVR* gene was then identified by isolating the human gene responsible for this transforming activity (53, 68). PVR, later designated CD155, is an integral transmembrane protein that has three immunoglobulin (Ig)-like domains and is encoded on chromosome 19.

The interaction between PV and PVR has been extensively investigated. The N-terminal Ig-like domain of PVR is responsible for PV binding (23, 54, 108). This domain penetrates the "canyon" that surrounds the five-fold protrusion on the capsid surface. The binding site involves all three major capsid proteins, VP1, VP2, and VP3. There are several critical amino acid residues in PVR for binding that have been identified by both mutational analyses (1, 4, 70) and cryo-electron microscopy (3, 33). Amino acid sequences of CD155 have been found to rapidly change during evolution. Of note, the critical amino acids in CD155 are not conserved in orthologs of nonsusceptible animal species (45, 50, 55).

Development of tg Animal Models

Soon after the isolation of the human *PVR* gene, attempts were made to generate tg mice, anticipating that the expression of human PVR would make nonsusceptible mice susceptible. Indeed, tg mice that

express the human *PVR* gene with its natural promoter are susceptible to PV infection (56, 57, 102). The infected mice exhibit clinical signs and pathological lesions that resemble human poliomyelitis after intracerebral, intraperitoneal, intravenous, intramuscular, or intranasal inoculation of PV (15, 56, 57, 75, 101, 102). Unlike humans, however, these tg mice are not susceptible to oral infection.

Despite the inability to orally infect tg mice, the development of mouse models has improved investigations of PV dissemination in an animal. In addition to monkeys, PVR-Tg21 mice are recognized by the World Health Organization as an animal model of poliomyelitis (19). tg mice have also been generated in which PVR is expressed under the control of artificial promoters, including cPVR mice with the β-actin promoter (15), fatty acid-binding protein (FABP)–PVR mice with the rat FABP promoter (118), and CAG-PVR mice with the CAG promoter (43). The tg mice have also made it possible to investigate the importance of host genes with respect to the pathogenesis of PV infections by crossing the tg mice with mice in which genes of interest have been modified.

PV REPLICATION IN THE GI TRACT: THE GI BARRIER

Site of Entry and Primary Multiplication

PV enters into the systemic circulation after ingestion of the virus. There are a number of structures that are important in understanding PV infection by the oral route. The majority of the epithelial cells lining the gastrointestinal (GI) tract form a tight barrier that is the first physical barrier for PV infection. A structure called the follicle-associated epithelium (FAE) is located in Peyer's patches above the lymphoid follicle and contains microfold (M) cells, which are capable of transporting molecules from the intestinal lumen into the underlying lymphoid cells (79, 90) (Fig. 2). The mechanism by which PV invades the lymphoid tissues is still unknown.

In humans, chimpanzees, and cynomolgus monkeys, which are susceptible to oral PV infection, a significant titer of PV initially appears in lymphatic tissues, such as the tonsils in the pharynx and Peyer's patches in the small intestine (9, 112); however,

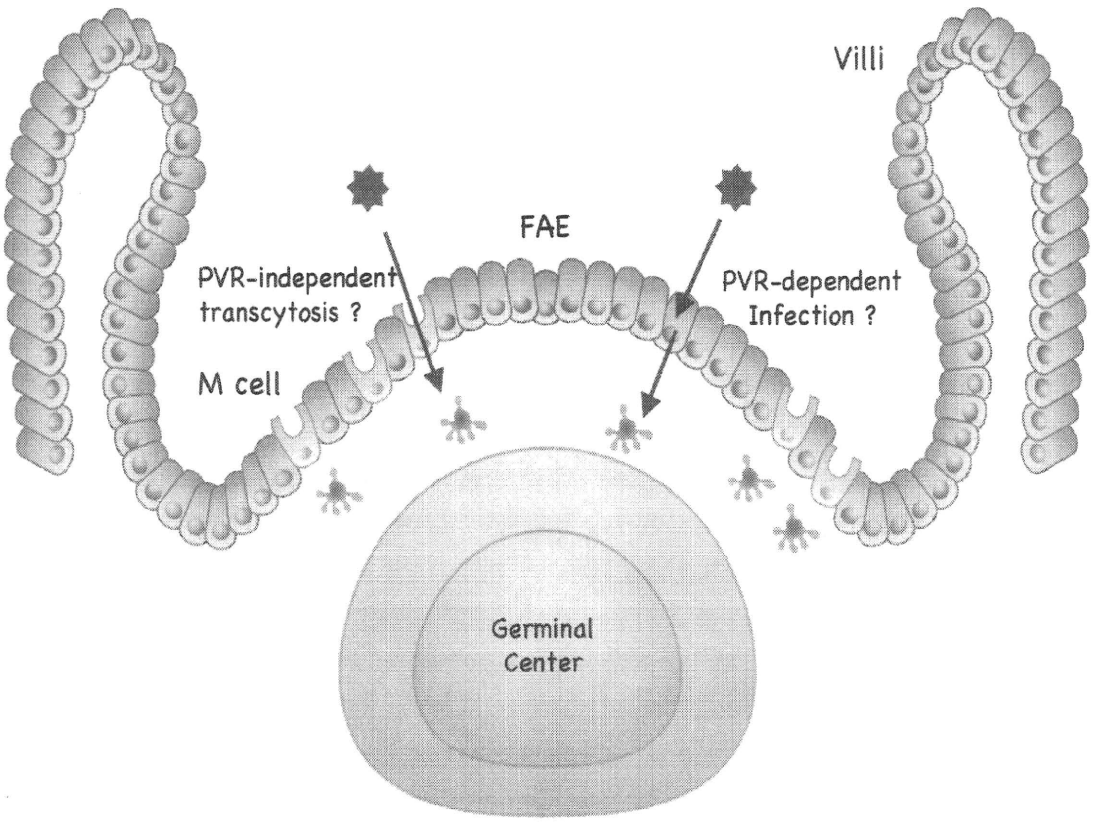

Figure 2. Structure of the GI tract barrier. The epithelial cells (enterocytes) lining the GI tract form a tight physical barrier for PV infection. A structure called FAE is present in Peyer's patches above the lymphoid follicle and contains M cells, which are capable of transporting molecules from the intestinal lumen into the underlying dendritic cells or macrophages. The primary replication sites of PV and the source of excreted virus have not yet been determined. It is also unknown whether PV replicates in the epithelial cells in a PVR-dependent manner or whether PV is incorporated via M cells by transcytosis without lytic infection.

specific histopathological lesions are not clearly correlated with these presumed sites of multiplication (8). Rhesus monkeys (39) and PVR tg mice are not susceptible by this route of infection (57, 102). Some researchers have conducted experiments to elucidate the mechanism by which PV enters the systemic circulation by comparing susceptible and nonsusceptible species; however, the experiments performed have generally been incomplete and with inconsistent results (see below) (46, 47, 89, 109, 110, 118). Therefore, it is still not known which types of cells are infected and how PV accesses lymphatic tissues.

One idea proposed is that PV invades epithelial cells and lymphatic tissues by a direct infection that depends on the expression of PVR. Kanamitsu et al. (47) infected cynomolgus monkeys with the Mahoney strain and, by using immunofluorescence analysis, observed viral replication in squamous epithelial cells and macrophages in the lymphatic structure of the tonsils. This result suggested that the entry of PV into lymphatic tissues is associated with replication in these cells. Iwasaki et al. (46) compared the sites of PVR expression in humans, rhesus monkeys, and PVR tg (PVR-Tg21) mice. They observed PVR expression in epithelia, including the FAE and M cells of Peyer's patches and the germinal center of the follicle in humans. In rhesus monkeys, however, PVR expression was low, while in PVR-tg mice, PVR was barely observable in epithelium and absent in germinal centers. Those authors hypothesized that PVR expression in these sites is important in establishing PV infection in the GI tract. These findings have not been confirmed by experiments involving PV infection. Zhang and Racaniello (118) considered that the resistance of PVR tg mice to oral injection was due to the absence of PVR expression in cells that are critical to support PV replication in this region. These investigators generated a new tg mouse that expressed PVR under the rat FABP promoter in order to test whether enhanced PVR expression in the epithelial cells would result in susceptibility to oral infection. The FABP-PVR mice did not become susceptible to oral infection; however, a detailed analysis of the Peyer's patch cells of the FABP-PVR mice and the expression of PVR were not reported, so it remains unclear whether PVR expression in this tissue is necessary for the establishment of oral infection.

Other reports support the entry of PV by transcytosis through M cells, as is the case with other pathogens. Electron microscopic analysis by Sicinski et al. (109) showed that PV adhered to the surface of M cells and vesicles and that PV was incorporated in the M cells on the FAE. In another report, Ouzilou et al. (89) cultured Caco-2 cells in the upper chamber of a transwell with freshly prepared lymphocytes in the lower chamber. The Caco-2 cells formed a layer sealed with tight junctions. Some cells in the layer differentiated into M-like cells, serving as an in vitro model of FAE. When PV was added to the upper chamber, intact PV was recovered within 2 h from the lower chamber, suggesting that PV can pass through the Caco-2 layer by transcytosis in M cells.

PV REPLICATION IN EXTRANEURAL TISSUES: THE INNATE IMMUNE BARRIER

Roles of PVR and IRES *trans*-Activating Factors

PV replicates in extraneural tissues during the viremic phase. In addition, PV can be recovered from extraneural tissues of orally infected chimpanzees and cynomolgus monkeys (9, 112) and from tg mice infected intravenously (44, 52); however, the amounts of PV recovered are relatively small. No pathological changes are discernible in these tissues. The results suggest that the extraneural tissues are not fully permissive to PV infection, in contrast to the extensive replication that occurs in the CNS. The reason for the extensive replication of PV in the CNS has not been elucidated. One possible hypothesis is that factors that support PV replication are expressed preferentially in the target tissues. Holland proposed that PVR is the determinant of PV tissue tropism (36); however, PVR expression is observed in a wider range of tissues, including resistant ones, suggesting that PVR is necessary but not the sole determinant of PV tropism (22, 57, 58, 68, 100).

It is known that the internal ribosome entry site (IRES) in the 5′ noncoding region (5′ NCR) can function in a tissue- and cell-type-specific manner. Pilipenko et al. (96) demonstrated that a chimeric Theiler's murine encephalomyelitis virus in which the 5′ NCR IRES was replaced by the corresponding region of foot-and-mouth disease virus (FMDV) was not able to replicate in the CNS. The FMDV IRES required a noncanonical translation initiation factor, IRES *trans*-activating factor 45, which is expressed in proliferating cells. This finding suggested that the tissue-specific replication ability of FMDV is controlled by a tissue-specific IRES activity that is mediated by a *trans*-acting factor with tissue-specific expression. Similarly, Gromeier et al. (27) and Yanagiya et al. (115) produced chimeric viruses between human rhinovirus and PV and between hepatitis C virus and PV, respectively. These chimeras lost the ability to replicate in the CNS, suggesting that the IRES of human

rhinovirus and hepatitis C virus is controlled in a tissue-specific manner and does not work in the CNS. However, Kauder and Racaniello (48) produced a recombinant adenovirus that had a bicistronic reporter with the PV IRES in the second cistron. The PV IRES mediated translation not only in the neural tissues but also in extraneural tissues. Thus, it is not likely that the PV IRES mediates preferential replication of PV in the CNS. As we will discuss later, the PV IRES has an important role in replication efficiency in the CNS.

Role of Interferon Response in Tissue Tropism

Ida-Hosonuma et al. (44) reported that a transient increase in PV titer was found in extraneural tissues of infected PVR tg mice. This finding prompted the investigators to speculate that the cells in extraneural tissues are also susceptible to PV and can initiate the replication process but that progression of the infection cascade was inhibited by an unknown mechanism. The reason for the inability of virus to efficiently replicate in extraneural tissues was clarified by experiments using mice deficient in the type I interferon (IFN) response. The results showed that PVR tg mice that were IFN-α/β receptor 1 (IFN-α/βR1) deficient (74) were highly susceptible to PV infection. Interestingly, in the absence of the normal IFN response, PV was able to replicate efficiently not only in the CNS but also in extraneural tissues, such as liver, spleen, and pancreas. The results suggested that extraneural tissues possess all the host factors required for PV replication but that an active host innate immune defense prevents viral replication in these sites. Of note, extraneural tissues express a higher basal activity of IFN-stimulated genes, even in the noninfected state, than neural tissues. In addition, the IFN response induced in response to PV infection in extraneural tissues is greater than in neural tissues.

This difference in the type I IFN response in the two tissues may be the reason for the differences in replication efficiency of PV. Furthermore, Ohka et al. (83) observed that PV replication in the small intestine was enhanced in IFN-α/βR1-deficient PVR tg mice. These results suggested that the IFN response can also act as a barrier to prevent PV replication in extraneural tissues (Fig. 3), constituting an innate immune barrier rather than a physical barrier. The

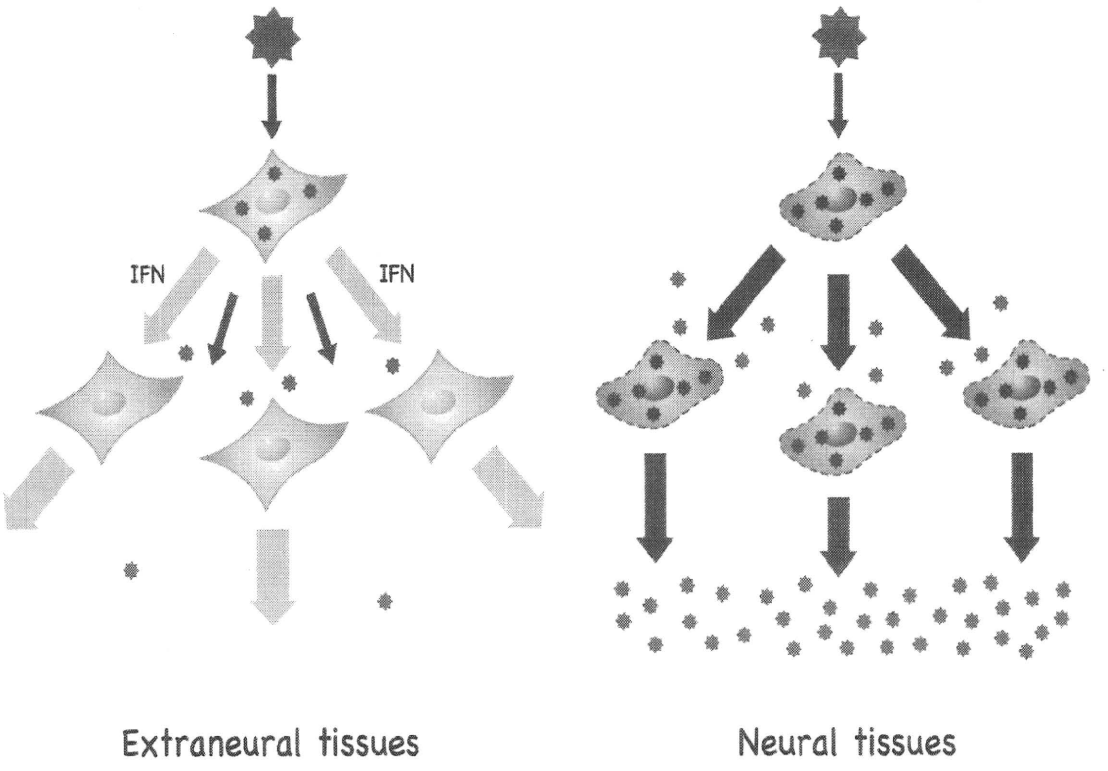

Figure 3. Innate immune barrier in extraneural tissues. Although many tissues are exposed to PV during the viremic phase, PV replication in the extraneural tissues is strongly suppressed by the innate immune response, which is mediated by type I IFN. Many cells in the extraneural tissues possess all of the host factors required for PV replication and have the potential to support PV replication. Soon after infection of a single cell, an active host innate immune defense induces an antiviral state in the surrounding cells and stops the cascade of viral infection in these sites. Thus, this response acts as an immunological barrier. In neural tissues, however, the innate immune response is less active than in the extraneural tissues, allowing a sequential cascade of viral infection.

barrier controls the permissiveness of extraneural tissues and keeps the levels of viremia low. This barrier may be the reason that PV invasion into the CNS occurs in less than 1% of infections, even in nonimmune individuals. In contrast, a relatively weak IFN response in the CNS permits PV replication once the virus reaches the CNS. Thus, the IFN response, which does not function equally in all tissues, is an important factor that determines the neurotropic nature of PV. The importance of the IFN response in protection of nontarget tissues has also been described for other virus infections (24, 71, 103, 113).

CNS ENTRY OF PV: HEMATOGENOUS AND NEURAL PATHWAYS

The CNS is isolated from the extraneural tissues. To date, at least two pathways by which PV invades the CNS are known: via the blood-brain barrier (BBB) and by retrograde axonal transport.

Penetration of the BBB

The BBB, which is composed of endothelial cells of blood vessels that are sealed together at their edges by tight junctions, does not allow free transport of materials, including pathogens, between the bloodstream and parenchyma of the CNS (25). Therefore, the BBB acts as a physical barrier to PV dissemination (Fig. 4); however, PV is believed to invade the CNS through the BBB.

Coyne et al. (14) showed that cultured human brain microvascular endothelial cells, which serve as an in vitro model of the BBB, are susceptible to PV infection. In addition, human endothelial cells from the umbilical vein become susceptible to PV after cultivation in vitro (13). These data, however, do not directly prove that endothelial cells are susceptible to in vivo PV infection, since it is known that cells derived from nonsusceptible tissues can acquire PV susceptibility to infection after cultivation in vitro (20, 117). Data from in vivo studies actually suggest that the invasion of the BBB by PV does not involve infection of endothelial cells. Yang et al. (116) performed a physiological pharmacokinetic analysis to investigate the fate of PV inoculated into the tail vein of mice. The inoculated virus was distributed to various tissues, such as the spleen, liver, kidney, small intestine, heart, lung, muscle, and CNS tissues. The amount of PV delivered to the CNS tissues was significantly greater than the theoretical amount estimated within the vascular volume. In contrast, the amount of PV distributed to other tissues almost equaled the theoretical amount predicted based on vascular volume. These data suggested that PV passes into the parenchyma of the CNS through the BBB. Of interest, the distribution profiles of the virus in tg and non-tg mice were similar, indicating that PVR expression in tg mice (and therefore infection of endothelial cells) does not play a significant role in the tissue distribution profile of PV. The rates of accumulation of the virus in the brain are more than 100 times higher than that of albumin (which is not thought to permeate the BBB via a specific transport system) and are similar to that of cationized rat serum albumin (which is known to efficiently permeate the BBB). The above data suggest that PV penetrates the BBB with a fairly high degree of efficiency, independent of expression of the PVR. Thus, it is possible that host cell molecules other than PVR are involved in the penetration of the BBB by PV. The precise mechanism by which PV entry into the CNS occurs remains to be elucidated.

Retrograde Axonal Transport

Another pathway leading to neural dissemination of PV is by means of retrograde axonal transport, which has been reported for humans, monkeys, and tg mice (Fig. 4). This pathway first drew attention during the Cutter vaccine incident (78), in which children received incompletely inactivated polio vaccine prepared from virulent PV strains; it was observed at that time that the initial paralysis was frequently seen in the inoculated limb. In addition, experimental evidence indicates that PV can spread to the CNS through the sciatic nerve of monkeys (77) and tg mice (101). Of note, there is also a correlation between muscle trauma during the viremic phase of PV infection and an increased risk of poliomyelitis (10), suggesting that the neural pathway is important in this phenomenon of "provocation poliomyelitis." Provocation poliomyelitis was experimentally reproduced in tg mice (28), with results that suggested that skeletal muscle injury stimulates retrograde axonal transport of PV and thereby facilitates viral invasion of the CNS, with resultant spinal cord damage. These findings renewed interest in studying the mechanism by which PV uses neural pathways to enter the CNS.

Mechanism of Axonal Transport of PV

Experiments involving transection of the sciatic nerve following intramuscular inoculation of PV into the calf of PVR tg mice demonstrated that some of the inoculated virus moves along the axon via retrograde

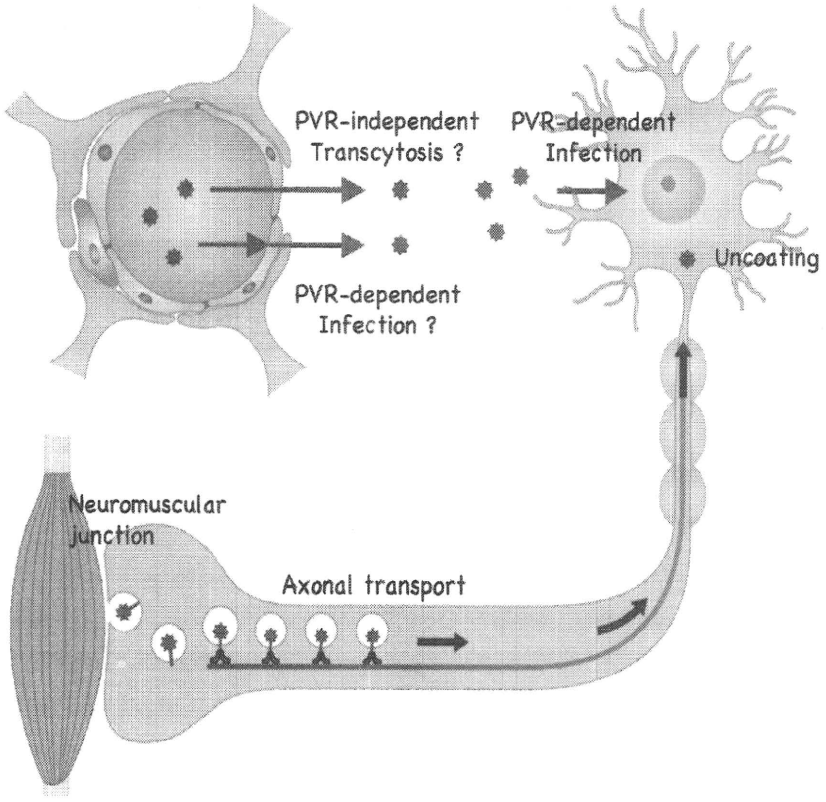

Figure 4. Two pathways of CNS invasion. PV is able to enter the CNS by at least two distinct pathways. One pathway involves the direct penetration of the BBB from the bloodstream into the parenchyma of the CNS. The BBB is composed of endothelial cells of blood vessels that are sealed together at their edges by tight junctions. Generally, it does not allow free transport of pathogens. There is no strong evidence that supports direct infection of endothelial cells. Physiological pharmacokinetic analysis suggests that the PV is able to permeate the BBB from the bloodstream into the parenchyma of the CNS independently of PVR. The precise mechanism by which PV employs this pathway remains to be elucidated. Another pathway leading to neural dissemination of PV is by retrograde axonal transport. PV is incorporated into endosomes by PVR-mediated endocytosis at neuromuscular junctions. The C-terminal cytoplasmic tail of the PVR on the surface of the endosome is able to bind TCTEL1 (in humans) or Tctex-1(in mice), which is the light chain-1 of the cytoplasmic dynein complex. PV-containing endosomes move on the microtubules along the axon via retrograde transport at a rate of more than 12 cm/day, a velocity classified as fast retrograde axonal transport. PV particles do not initiate conformational changes during transport along the axon until they reach the cell body of the neuron.

transport at a rate of more than 12 cm/day (87), a velocity seen with fast retrograde axonal transport (12). These results suggested that PV is packed in endosomes during transport through the axon, since this is the case with many substances that are carried via retrograde transport by the fast transport system. Indeed, an electron microscopic study detected endosomes containing PV at the neuromuscular junction in the vicinity of the inoculation site. Thus, it is possible that PV is within endosomes that result from PVR-mediated endocytosis of the virus at synapses and are then conveyed via retrograde transport through the axon (84).

The majority of PV-related materials in the sciatic nerve showed a sedimentation coefficient of 160S, suggesting that the PV is conveyed without conformational change in the axon and initiates the uncoating step after reaching the cell body of the neurons (87). Of interest, a human homolog (TCTEL1) of mouse Tctex-1, which is the light chain-1 of the cytoplasmic dynein complex (a complex that uses microtubules as pathways for transport), has been reported to bind the cytoplasmic domain of PVR (72, 84). In addition, treatment of the sciatic nerve with the microtubule-depolymerizing agent vinblastine results in slower retrograde transport of the virus to the spinal cord of tg mice (84). It is possible that PV inoculated intramuscularly is incorporated into cells by PVR-mediated endocytosis at synapses, without any PVR-mediated conformational changes of the virion particle. The cytoplasmic domain of PVR on the surface of the endosomes that enclosed the poliovirion could then interact with cytoplasmic dynein, and the endosomes could be retrograde transported